

Rigidified Derivative of the Non-macrocyclic Ligand H₄OCTAPA for Stable Lanthanide(III) Complexation

Fátima Lucio-Martínez, Zoltán Garda, Balázs Váradi, Ferenc Krisztián Kálmán, David Esteban-Gómez, Éva Tóth, Gyula Tircsó,* and Carlos Platas-Iglesias*



Cite This: *Inorg. Chem.* 2022, 61, 5157–5171



Read Online

ACCESS |



Metrics & More

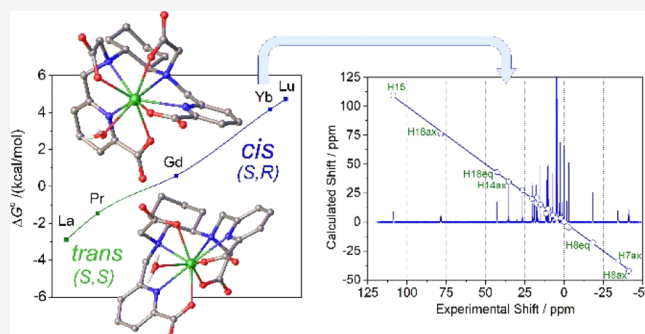


Article Recommendations



Supporting Information

ABSTRACT: The stability constants of lanthanide complexes with the potentially octadentate ligand CHXOCTAPA⁴⁻, which contains a rigid 1,2-diaminocyclohexane scaffold functionalized with two acetate and two picolinate pendant arms, reveal the formation of stable complexes [$\log K_{LaL} = 17.82(1)$ and $\log K_{YbL} = 19.65(1)$]. Luminescence studies on the Eu³⁺ and Tb³⁺ analogues evidenced rather high emission quantum yields of 3.4 and 11%, respectively. The emission lifetimes recorded in H₂O and D₂O solutions indicate the presence of a water molecule coordinated to the metal ion. ¹H nuclear magnetic relaxation dispersion profiles and ¹⁷O NMR chemical shift and relaxation measurements point to a rather low water exchange rate of the coordinated water molecule ($k_{ex}^{298} = 1.58 \times 10^6 \text{ s}^{-1}$) and relatively high relaxivities of 5.6 and 4.5 mM⁻¹ s⁻¹ at 20 MHz and 25 and 37 °C, respectively. Density functional theory calculations and analysis of the paramagnetic shifts induced by Yb³⁺ indicate that the complexes adopt an unprecedented cis geometry with the two picolinate groups situated on the same side of the coordination sphere. Dissociation kinetics experiments were conducted by investigating the exchange reactions of LuL occurring with Cu²⁺. The results confirmed the beneficial effect of the rigid cyclohexyl group on the inertness of the Lu³⁺ complex. Complex dissociation occurs following proton- and metal-assisted pathways. The latter is relatively efficient at neutral pH, thanks to the formation of a heterodinuclear hydroxo complex.



INTRODUCTION

Stable complexation of lanthanide ions (Ln³⁺) in aqueous solution is a coordination chemistry problem that has received much attention in the last 3 decades. This interest is related to a great extent to the important medical and biomedical properties of some lanthanide complexes, which include (1) the use of Gd³⁺ complexes as contrast agents in magnetic resonance imaging (MRI),^{1–5} (2) the potential of luminescent Ln³⁺ complexes, particularly Eu³⁺ and Tb³⁺, in optical imaging and bioanalytical applications,^{6–8} and (3) the interesting properties of radioisotopes in the lanthanide series (i.e., ¹⁷⁷Lu) for radiopharmaceutical applications.^{9,10} All these applications require stable complexation of metal ions and slow dissociation kinetics to avoid undesirable effects (toxicity issues).^{11,12} Furthermore, the application of Ln³⁺ complexes as radiopharmaceuticals requires a fast complexation of the radioisotope under mild conditions.¹³ Chelates for the preparation of efficient luminescent complexes must contain chromophore units suitable for indirect excitation of the relevant Ln³⁺ excited state, while protecting the metal ion from the vibrational quenching associated to the coordination of water molecules.¹⁴

The chelates used for stable Ln³⁺ complexes are often either macrocyclic or non-macrocyclic systems containing hard

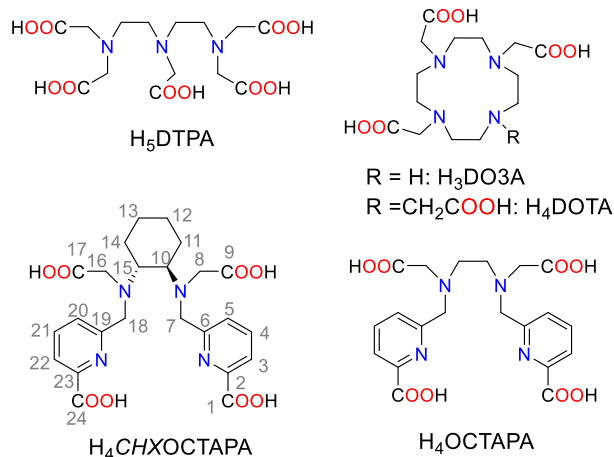
carboxylate or phosphonate donor groups whose denticity ranges from 7 to 10.^{15–17} Ligands with lower denticity like EDTA result in complexes endowed with low stability,¹⁸ while octa- or nonadentate ligands generally present favorable complexation properties.^{19,20} Macrocyclic ligands often form complexes with superior thermodynamic stability and exceptional kinetic inertness,²¹ but in some cases lead to very slow complexation kinetics.^{21–24} On the other hand, non-macrocyclic ligands such as DTPA⁵⁻ (Chart 1) and DTPA bisamides often present faster dissociation kinetics, which is problematic for medical applications.^{11,25} Gd³⁺ complexes with DTPA bisamides were considered to have superior kinetic inertness than the DTPA⁵⁻ analogue. However, more recent studies demonstrated that different anions present in vivo catalyze the dissociation of Gd³⁺ complexes with DTPA bisamides.¹¹

Received: February 14, 2022

Published: March 11, 2022



Chart 1. Ligands Discussed in the Present Work



In 2004, we reported the potentially octadentate ligand H_4OCTAPA (Chart 1), whose Gd^{3+} complex was originally designed as a potential MRI contrast agent candidate.²⁶ This study demonstrated the presence of a water molecule in the inner coordination sphere. Subsequent investigations performed by Mazzanti,^{27,28} Orvig,^{29,30} and our own group³¹ pointed to a high thermodynamic stability of the lanthanide complexes, which, however, exhibit fast dissociation kinetics. Orvig and co-workers showed that OCTAPA presents very promising properties for the development of ^{111}In , ^{90}Y , and ^{177}Lu radiopharmaceuticals.^{32,33} Bifunctional derivatives of H_4OCTAPA were also reported and successfully tested in vivo upon radiolabeling with these radioisotopes.^{34–36} The rigidified ligand CHXOCTAPA^{4-} (also known as $\text{H}_4\text{CDDADPA}^{4-}$) was reported almost simultaneously by the group of Orvig and us.^{37,38} The corresponding Gd^{3+} complex is remarkably inert with respect to dissociation, with dissociation rate constants comparable to those of macrocyclic complexes such as $[\text{Gd}(\text{DO3A})]$.

In this paper, we present a detailed characterization of the Ln^{3+} complexes of CHXOCTAPA using a wide range of experimental and computational techniques. A multinuclear (^1H and ^{13}C) NMR study and density functional theory (DFT) calculations were used to establish the structure of the complexes in solution, including the analysis of the paramagnetic Yb^{3+} -induced ^1H NMR shifts. These studies revealed unexpected features of the structure in solution of these complexes. We also present a full characterization of the relaxometric properties of the Gd^{3+} complex involving ^1H nuclear magnetic relaxation dispersion (NMRD) studies and ^{17}O NMR chemical shifts and relaxation rates. A detailed analysis of the photophysical properties of the Eu^{3+} and Tb^{3+} complexes, including quantum yield determination, is reported. Finally, we also determined the stability of some of the complexes across the lanthanide series and assessed their kinetics of dissociation. The stabilities of the complexes formed with divalent metal ions of biological relevance are also reported.

RESULTS AND DISCUSSION

Stability of the Ln^{3+} Complexes. Stability constant determination requires measuring the protonation constants of the ligand using the same electrolyte background. The protonation constants of CHXOCTAPA^{4-} in 0.15 M NaCl

reported previously by Orvig³⁷ and us³⁸ were in good agreement, though slight discrepancies can be noticed for $\log K_5^{\text{H}}$ and $\log K_6^{\text{H}}$ (Table S1, Supporting Information). These protonation processes take place in the pH range where complex dissociation occurs, and thus the accurate determination of their values is critical for determining stability constants. We therefore performed new potentiometric titrations using a higher ligand concentration (4.38 mM) in the pH range 1.65–11.95, which allows for a more accurate estimation of protonation constants (Figure S30, Supporting Information). These experiments yielded $\log K_5^{\text{H}} = 1.59(1)$ and $\log K_6^{\text{H}} = 0.61(4)$.

The stability of the Gd^{3+} complex with CHXOCTAPA^{4-} was reported in a previous paper.³⁸ This complex was found to be nearly fully formed at $\text{pH} \sim 2$, which complicates stability constant determination using potentiometric titrations. The stability of the complex could be determined using the relaxometric method with aqueous solutions buffered with dimethylpiperazine (DMP).³⁹ Relaxivity, r_{1p} , refers to the paramagnetic longitudinal relaxation rate enhancement of water protons for a 1 mM concentration of the paramagnetic Gd^{3+} ion.⁴⁰ The relaxivity of $[\text{Gd}(\text{H}_2\text{O})_8]^{3+}$ is considerably higher than that of the $[\text{Gd}(\text{CHXOCTAPA})]^-$ complex, and thus complex dissociation provoked by the addition of competing metal ions (La^{3+} , Yb^{3+} , or Zn^{2+}) causes an important increase of the relaxation rate of water protons (Figure 1). These experiments were carried out using the batch

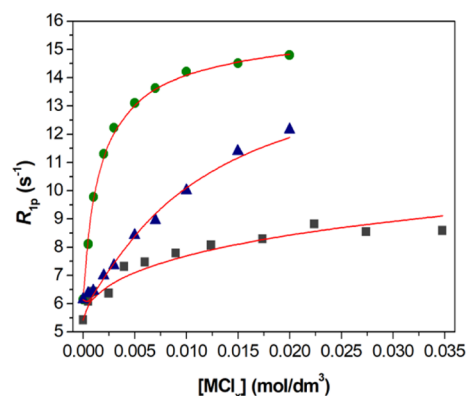


Figure 1. Relaxometric titrations (25 °C, 0.15 M NaCl) of the $[\text{Gd}(\text{CHXOCTAPA})]^-$ complex with LaCl_3 (squares, $c_{\text{Lig}} = c_{\text{Gd}^{3+}} = 1.001$ mM at $\text{pH} = 4.69$), YbCl_3 (circles, $c_{\text{Lig}} = c_{\text{Gd}^{3+}} = 1.113$ mM at $\text{pH} = 4.79$), and ZnCl_2 (triangles, $c_{\text{Lig}} = c_{\text{Gd}^{3+}} = 1.001$ mM at $\text{pH} = 4.81$). All solutions were buffered using 50 mM DMP. The solid lines show the fit of the data for stability constant determination.

method and long equilibration times (4 weeks) to ensure that thermodynamic equilibrium was attained. The titration profiles observed for La^{3+} and Yb^{3+} are remarkably different, with addition of Yb^{3+} inducing a rather sharp inflection point. This anticipates that the stability of the Yb^{3+} complex is slightly higher than that of the La^{3+} analogue. The fit of the relaxation data confirms this qualitative analysis, yielding stability constants of $\log K_{\text{YbL}} = 19.60(5)$ and $\log K_{\text{LaL}} = 18.09(3)$.

The stability of the complexes with CHXOCTAPA^{4-} experiences a slight increase from La^{3+} to Gd^{3+} as the charge density of the metal ion increases. This is the most common trend observed for Ln^{3+} complexes,⁴¹ though it is often more pronounced than observed here.¹⁹ Only a few cases of reversed stability were reported for the complexes of macrocyclic

Table 1. Protonation and Stability Constants of the Metal Complexes Formed with CHXOCTAPA⁴⁻ and Related Ligands (25 °C, 0.15 M NaCl)

	CHXOCTAPA ⁴⁻	OCTAPA ^{4-a}	DTPA ⁵⁻	DO3A ^{3-g}	DOTA ⁴⁻
log <i>K</i> _{LaL}	17.82(1); 18.09(3) ^k	19.92	19.49 ^e	18.63	21.7 ⁱ
log <i>K</i> _{LaHL}	2.00(1)		2.60 ^e		
log <i>K</i> _{LaH-1L}	12.75(4)				
log <i>K</i> _{GdL}	19.92(1)	20.23	22.03 ^d /22.46 ^e	21.56/19.06 ^h	24.7 ⁱ
log <i>K</i> _{GdHL}	1.02(4)		1.96 ^d /2.39 ^e		
log <i>K</i> _{GdH-1L}	12.45(2)				
log <i>K</i> _{YbL}	19.65(1), 19.60(5) ^k	19.90 ^b			
log <i>K</i> _{YbHL}	1.89(2)				
log <i>K</i> _{YbH-1L}	12.24(2)				
log <i>K</i> _{LuL}		20.49/20.08 ^c	22.44 ^e	21.44	25.4 ⁱ
log <i>K</i> _{LuHL}			2.18 ^e		
log <i>K</i> _{MgL}	5.96(1)	6.12	9.27 ^e	11.64	11.49 ^g
log <i>K</i> _{MgHL}	6.03(3)	5.24	6.85 ^e		
log <i>K</i> _{MgH2L}		4.54			
log <i>K</i> _{CaL}	8.42(2)	9.55/9.4	10.7 ^f	12.57	16.11 ^g
log <i>K</i> _{CaHL}	4.83(5)	3.92	6.11 ^f	4.60	
log <i>K</i> _{CaH2L}	4.57(6)	2.56			
log <i>K</i> _{Ca2L}	3.88(7)	1.55			
log <i>K</i> _{ZnL}	16.97(3)	18.91	17.58 ^d	21.57	20.21 ^g
log <i>K</i> _{ZnHL}	4.04(3)	3.91	5.37 ^d	3.47	
log <i>K</i> _{ZnH2L}	3.15(2)	3.54	2.38 ^d	2.07	
log <i>K</i> _{ZnH3L}	1.34(4)				
log <i>K</i> _{ZnH-1L}	11.63(7)				
log <i>K</i> _{Zn2L}	3.99(5)	2.3	4.33 ^d		
log <i>K</i> _{Zn2HL}	3.26(4)				
log <i>K</i> _{Zn2L(OH)}	7.63(4)				
log <i>K</i> _{Zn2L(OH)2}	8.39(2)				
log <i>K</i> _{CuL}	20.76(6) ^j	22.08	23.40 ^d	25.75	24.83 ^g
log <i>K</i> _{CuHL}	4.02(9) ^j	3.95	4.63 ^d	3.65	
log <i>K</i> _{CuH2L}	4.07(2) ^j	3.21	2.67 ^d	1.69	
log <i>K</i> _{CuH3L}			2.03 ^d		
log <i>K</i> _{CuH-1L}	12.26(5) ^j				
log <i>K</i> _{Cu2L}	5.64(6) ^j	3.2	6.56 ^d		
log <i>K</i> _{Cu2HL}	3.33(6) ^j		2.20 ^d		
log <i>K</i> _{Cu2L(OH)}	7.80(11) ^j				
log <i>K</i> _{Cu2L(OH)2}	9.10(11) ^j				

^aData from ref 31 in 0.15 M NaCl unless otherwise indicated. ^bData in 0.16 M NaCl from ref 29. ^cData from ref 34. ^dData in 0.15 M NaCl from ref 20. ^eData in 0.1 M KCl from ref 45. ^fData in 0.1 M NaCl from ref 45. ^gData in 0.1 M KCl from ref 47 unless otherwise stated. ^hData in 0.15 M NaCl from ref 48. ⁱData in 0.1 M NaCl from ref 49. ^jData obtained by simultaneous fitting of UV-vis and pH-potentiometry titration data obtained at 1:1 and 2:1 metal-to-ligand ratio. ^kDetermined using relaxometric titrations.

ligands.⁴²⁻⁴⁴ The complexes with Gd³⁺ and Yb³⁺ present very similar stability. The complexes with DTPA⁵⁻ present a similar trend, with an initial increase in stability for the light lanthanide ions, the stability constants becoming nearly constant for the heaviest lanthanides (Table 1).^{20,45}

The stability constants determined for the Ln³⁺ complexes of CHXOCTAPA⁴⁻ by different methods (pH-potentiometry and ¹H-relaxometry) are in excellent agreement, being comparable with those reported for the analogues with OCTAPA⁴⁻ (Table 1).^{29,31} This indicates that the replacement of the ethylenediamine spacer by a more rigid cyclohexyl group does not have a significant impact on complex stability, as observed recently for uranyl complexes.⁴⁶ The stability constants characterizing the Ln³⁺ complexes of CHXOCTAPA⁴⁻ are similar to those of DO3A³⁻,^{47,48} but remain lower than those reported for the analogous DOTA⁴⁻ complexes.^{47,49} We note that the stability constants determined in 0.1 M KCl and 0.15 M NaCl for the Gd³⁺ complex of DTPA⁵⁻ are in good agreement, while there is

a significant difference in the case of DO3A³⁻. This shows that Na⁺ cations form a relatively stable complex with DO3A³⁻ derivatives.⁴⁸

Potentiometric titrations using a high ligand concentration (4.38 mM) in the presence of equimolar concentrations of La³⁺, Gd³⁺, and Yb³⁺ allowed for determining stability and protonation constants of the metal complexes. The log *K*_{LnL} values obtained for the La³⁺ and Yb³⁺ complexes are in excellent agreement with those obtained by relaxometry. These experiments afforded also the protonation constant of the complexes and also evidenced the formation of hydroxo complexes at high pH (log *K*_{LnH-1L} > 12, Figures S7 and S8). For Gd³⁺, the stability constant determined by potentiometry log *K*_{GdL} = 19.92(1) is slightly lower than that obtained previously by relaxometry (log *K*_{GdL} = 20.68).³⁸ This slight discrepancy is related to the different set of ligand protonation constants used in the analysis.

The stability constants of the Mg^{2+} and Ca^{2+} complexes of CHXOCTAPA^{4-} could be determined using direct potentiometric titrations. Both cations form different protonated complex species in solution. Similarly, potentiometric titrations, using both 1:1 and 1:2 (M/L) stoichiometric ratios, allowed for determining the protonation constants of the complexes formed with Zn^{2+} and Cu^{2+} . These metal ions also form relatively stable dinuclear complexes characterized by the corresponding equilibrium constants K_{M2L} and different hydroxo complexes at basic pH, yielding rather complex species distributions in solution (Table 1; see also Figures S1–S8, Supporting Information).

The stability constant of the Zn^{2+} and Cu^{2+} complexes is too high to be determined using direct pH potentiometric titrations, and thus UV–vis spectrophotometric experiments were carried out under acidic pH to determine the stability of the Cu^{2+} complex, following the changes of the d–d absorption band at ca. 710 nm with pH (Figure S9, Supporting Information). The stability of the Zn^{2+} complex was obtained by competition titration with Gd^{3+} using relaxometry. The log K_{ML} values characterizing the formation of the Ca^{2+} , Zn^{2+} and Cu^{2+} complexes with CHXOCTAPA^{4-} are 1–2 log K units lower than those of the corresponding complexes formed with OCTAPA^{4-} . This is in contrast to previous studies, which evidenced a gain in complex stability with small metal ions upon incorporation of rigid cyclohexyl groups.⁵⁵ This imparts CHXOCTAPA^{4-} with a higher selectivity for the Ln^{3+} ions than OCTAPA^{4-} over potentially competing divalent metal ions in vivo.

Photophysical Properties. Ligands containing picolinate moieties were found to act as rather efficient sensitizers of the luminescent emission of Eu^{3+} and particularly Tb^{3+} .^{56–59} Furthermore, picolinate units can be easily functionalized to tune their photophysical properties and provide efficient two-photon absorption.^{60–62} Thus, we have investigated the emission spectra of the $[\text{Ln}(\text{CHXOCTAPA})]^-$ ($\text{Ln} = \text{Eu}, \text{Tb}$) complexes in aqueous solution. The emission spectrum of the Eu^{3+} complex is dominated by the ${}^5\text{D}_0 \rightarrow {}^7\text{F}_2$ ($\Delta J = 2$) transition and presents a rather intense ${}^5\text{D}_0 \rightarrow {}^7\text{F}_0$ transition (Figure 2). This spectral pattern is typical of Eu^{3+} in a coordination environment with a low symmetry.⁶³ The lifetime of the excited ${}^5\text{D}_0$ state measured in H_2O solution (598 μs) is typical of Eu^{3+} complexes containing one coordinated water molecule ($q = 1$). Lifetime measurements recorded in D_2O solutions afford a much longer lifetime of 2363 μs , as would be

expected considering the efficient vibrational quenching of Eu^{3+} luminescence provoked by O–H oscillators of coordinated water molecules.⁵⁰ The use of the empirical relationship proposed by Horrocks gives a q value of 1.0 ± 0.1 , confirming the presence of a water molecule coordinated to the metal center (Table 2).⁵⁰

The emission spectrum recorded for the Tb^{3+} complex presents the ${}^5\text{D}_4 \rightarrow {}^7\text{F}_J$ transitions expected for this metal ion, with J ranging from 6 to 3 (Figure S11, Supporting Information). The emission lifetimes of the excited ${}^5\text{D}_4$ state recorded in H_2O and D_2O provide a q value of 1.3,⁵¹ in agreement with the results obtained for Eu^{3+} .

The emission quantum yields measured for the Eu^{3+} (3.4%) and Tb^{3+} (11%) complexes were obtained using the corresponding trispicolinate complexes as secondary standards^{52,53} and are within the normal range reported for monohydrated chelates containing picolinate units.^{56,64,65} Thus, it is surprising that quantum yields one order of magnitude lower were reported by Platas-Iglesias et al. for the OCTAPA^{4-} analogues using quinine sulfate as standard (0.3 and 1.9% for Eu^{3+} and Tb^{3+} respectively).²⁶ Furthermore, higher quantum yields for the latter complexes were presented in a PhD thesis,⁶⁶ suggesting that the values reported by Platas-Iglesias were incorrect. We therefore reexamined the photophysical properties of the complexes with OCTAPA^{4-} (Table 2). These studies confirmed that the emission quantum yields of the Eu^{3+} and Tb^{3+} complexes with CHXOCTAPA^{4-} and OCTAPA^{4-} are very similar. The emission lifetimes measured for the two families of complexes are also very close, confirming the formation of $q = 1$ species in solution. The emission spectra recorded for the two Eu^{3+} complexes are rather similar, with a comparable splitting of the magnetic dipole ${}^5\text{D}_0 \rightarrow {}^7\text{F}_1$ transition ($\sim 140 \text{ cm}^{-1}$). We notice that the hypersensitive $\Delta J = 2$ transition is more intense in OCTAPA^{4-} than in CHXOCTAPA^{4-} , while the intensity of the magnetic dipole $\Delta J = 1$ transition remains very similar (Figure 2). This results in $\Delta J = 2/\Delta J = 1$ intensity ratios of 2.6 and 2.9 for the complexes with CHXOCTAPA^{4-} and OCTAPA^{4-} , respectively. It has been shown that the relative intensity of these transitions is very sensitive to changes in the metal coordination environment.^{67,68} Because the nature of the donor atoms and the number of coordinated water molecules is identical in the two complexes, these results suggest that the two complexes are characterized by somewhat different coordination polyhedra.

Further insights into the sensitization efficiency of Eu^{3+} by the picolinate chromophores can be gathered by applying the methodology developed by Werts,⁵⁴ which allows for estimating the radiative lifetime of the Eu^{3+} -centered emission τ_{Rad} , the metal-centered emission quantum yield Φ_{Eu} and the efficiency of the sensitization process η_{sen} (Table 2). The results of this analysis show that the observed emission quantum yields are limited by rather low Φ_{Eu} values associated to the quenching effect of the coordinated water molecule and a modest sensitization efficiency.^{69–71}

Structure of the Ln^{3+} Complexes in Solution. The structure of the $[\text{Ln}(\text{CHXOCTAPA})]^-$ complexes was investigated in D_2O solutions at pH 7.0 using ${}^1\text{H}$ and ${}^{13}\text{C}$ NMR spectroscopy. We initiated the study by examining the NMR spectra of the diamagnetic La^{3+} and Lu^{3+} complexes. The spectra of the Lu^{3+} complex are consistent with the presence of a main isomer in solution and a C_1 symmetry, as it shows 24 proton resonances and the same number of carbon

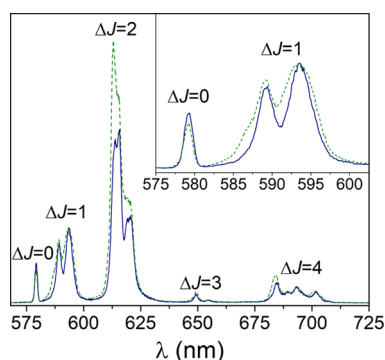


Figure 2. Emission spectra of the Eu^{3+} complexes with CHXOCTAPA^{4-} (blue solid line) and OCTAPA^{4-} (green dashed line) recorded in H_2O solution at pH 7.1 ($\lambda_{\text{ex}} = 279 \text{ nm}$; absorption and emission slits 1 nm, 10^{-4} M).

Table 2. Spectroscopic Properties of $[\text{Ln}(\text{CHXOCTAPA})]^-$ and $[\text{Ln}(\text{OCTAPA})]^-$ Complexes Measured in Aqueous Solutions (pH 7.1)^c

	$[\text{Eu}(\text{CHXOCTAPA})]^-$	$[\text{Eu}(\text{OCTAPA})]^-$	$[\text{Tb}(\text{CHXOCTAPA})]^-$	$[\text{Tb}(\text{OCTAPA})]^-$
$\lambda_{\text{max}}/\text{nm}$	272	272	271	272
$\epsilon/\text{M}^{-1} \text{cm}^{-1}$	7.66×10^3	7.50×10^3	8.34×10^3	9.36×10^3
$\tau_{\text{H}_2\text{O}}/\text{ms}^{\text{a}}$	0.598	0.584	1.527	1.473
$\tau_{\text{D}_2\text{O}}/\text{ms}^{\text{a}}$	2.363	2.292	2.822	2.863
$\Phi_{\text{H}_2\text{O}}/\%^{\text{b}}$	3.4	4.5	11	12
Q	1.0	1.1	1.3	1.2
$\tau_{\text{Rad}}/\text{ms}$	6.57	6.07		
$\Phi_{\text{Eu}}/\%$	9.60	9.10		
η_{sens}	0.37	0.47		

^a $\lambda_{\text{exc}} = 279 \text{ nm}$, estimated error $\pm 5\%$; $q_{\text{Eu}} = 1.11(\Delta k_{\text{obs}} - 0.31)$, ref 50; $q_{\text{Tb}} = 5.0(\Delta k_{\text{obs}} - 0.06)$, ref 51, with $(\Delta k_{\text{obs}} = 1/\tau_{\text{H}_2\text{O}} - 1/\tau_{\text{D}_2\text{O}})$.

^bDetermined using the trispicolinate complexes as standard, refs 52 and 53, $\lambda_{\text{exc}} = 279 \text{ nm}$, estimated error $\pm 15\%$. ^cDetermined according to ref 54.

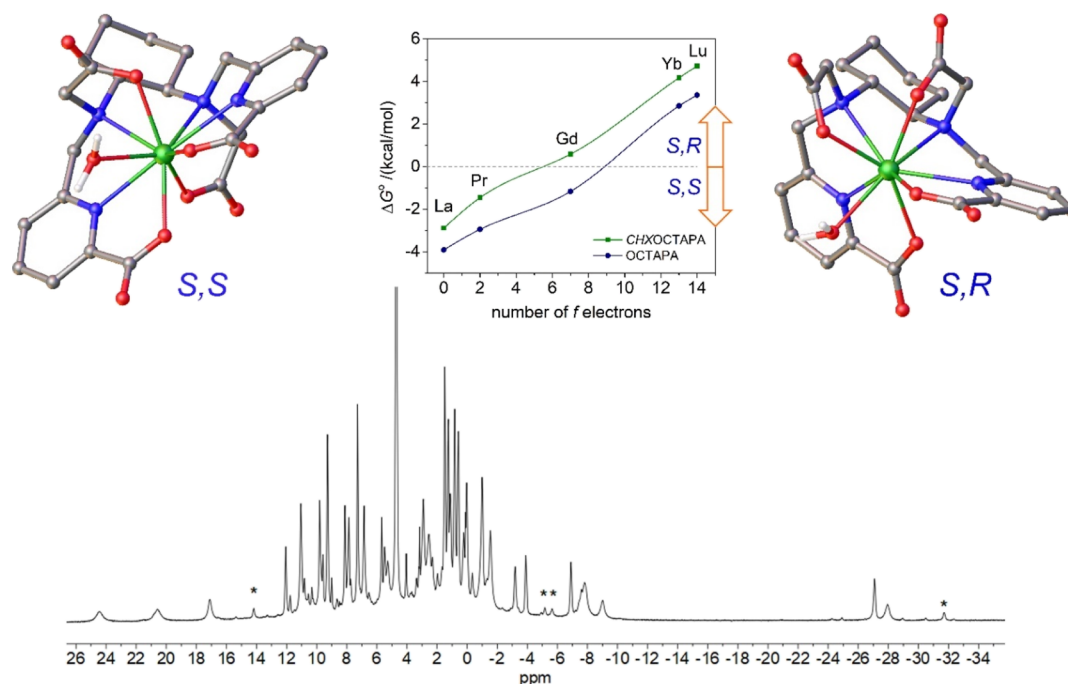


Figure 3. Top: Structures of the two isomers of $[\text{Gd}(\text{CHXOCTAPA})(\text{H}_2\text{O})]^- \cdot 2\text{H}_2\text{O}$ (second-sphere water molecules omitted for clarity) and relative energies calculated across the lanthanide series for the complexes with CHXOCTAPA^{4-} and OCTAPA^{4-} . Bottom: ^1H NMR spectrum of the Ce^{3+} complex recorded in D_2O solution (300 MHz, 25 °C, pH 7.0). Asterisks denote a minor species present in solution.

signals (Figure S20, Supporting Information). A full attribution of the NMR data was attained with the aid of 2D COSY, HSQC, and HMBC experiments (Table S2, Supporting Information). The spectrum points to a rigid structure of the complex in solution, as the ^1H spectrum displays well-resolved AB spin systems for the methylene protons. The spectra of the La^{3+} complex are, however, more complicated, evidencing the presence of two isomers in solution with very similar populations.

The ^1H NMR spectrum of the paramagnetic Ce^{3+} complex presents paramagnetically shifted signals in the approximate range 25 to -35 ppm (Figure 3). The spectrum is consistent with the presence of two isomers in solution, while only one isomer was observed previously for the Eu^{3+} complex.³⁸ All together, these results indicate that the complexes of the large lanthanide ions ($\text{La}-\text{Ce}$) are present in solution in the form of two diastereoisomers, while only one isomer is observed for Eu^{3+} and the heavier Ln^{3+} ions. DFT calculations were performed to understand the nature of the two diaster-

eoisomers present in solution for the $[\text{Ln}(\text{CHXOCTAPA})]^-$ complexes. A careful exploration of the potential energy surface provided two minimum energy geometries with rather small energy differences (Figure 3). These two minimum energy structures differ in the arrangement of the picolinate and acetate groups. One of the structures is characterized by nearly linear angles defined by the two pyridyl N atoms and the metal ion ($\text{N}_{\text{PY}}-\text{Ln}-\text{N}_{\text{PY}}$, $\sim 170^\circ$) and has been denoted as the trans isomer. Conversely, the second isomer (cis) is characterized by the coordination of picolinate (and acetate) groups on the same side of the metal ions, resulting in $\text{N}_{\text{PY}}-\text{Ln}-\text{N}_{\text{PY}}$ angles of $\sim 120^\circ$. The trans isomer is the most stable one at the beginning of the lanthanide series ($\text{La}-\text{Pr}$), while the cis isomer is predicted to be more stable for the second part of the lanthanide series ($\text{Gd}-\text{Lu}$). Analogous calculations performed for the $[\text{Ln}(\text{OCTAPA})]^-$ complexes provide a similar trend for the relative energies, though the cis isomer is stabilized later on along the series. As a result, our calculations predict that the most stable form for the $[\text{Gd}(\text{OCTAPA})]^-$ complex is the

trans isomer, which is in nice agreement with the X-ray structure reported by Mazzanti.²⁷ A trans structure was also established for the light Ln³⁺ complexes with OCTAPA⁴⁻ by analysis of the paramagnetic ¹H NMR shifts.²⁶ The cis isomer is characterized by different configurations of the amine N atoms (S,R or R,S), while these N atoms have the same configuration in the trans isomer (S,S or R,R, Figure 3).

The ¹H NMR spectra of Yb³⁺ complexes encode structural information that can be used to validate structural models obtained with DFT calculations.⁷² The ¹H NMR signals due to ligand nuclei in paramagnetic Yb³⁺ complexes experience large frequency shifts induced by the pseudocontact mechanism (δ^{PC}), which is related to the anisotropy of the magnetic susceptibility associated to the 4f electrons.^{73,74} The pseudocontact shift can be expressed as in eq 1 when the reference frame coincides with the principal directions of the magnetic susceptibility tensor χ

$$\delta^{\text{PC}} = \frac{1}{12\pi r^3} \left[\Delta\chi_{\text{ax}} \left(\frac{2z^2 - x^2 - y^2}{r^2} \right) + \frac{3}{2} \Delta\chi_{\text{rh}} \left(\frac{x^2 - y^2}{r^2} \right) \right] \quad (1)$$

where $r^2 = x^2 + y^2 + z^2$, x , y , and z are the Cartesian coordinates of a nucleus i relative to the location of a Yb³⁺ ion placed at the origin, and $\Delta\chi_{\text{ax}}$ and $\Delta\chi_{\text{rh}}$ are the axial and rhombic parameters of the symmetric magnetic susceptibility tensor.

The ¹H NMR spectrum of the Yb³⁺ complex of CHXOCTAPA is well resolved, presenting paramagnetically shifted resonances in the range +109 to -41 ppm (Figure 4).

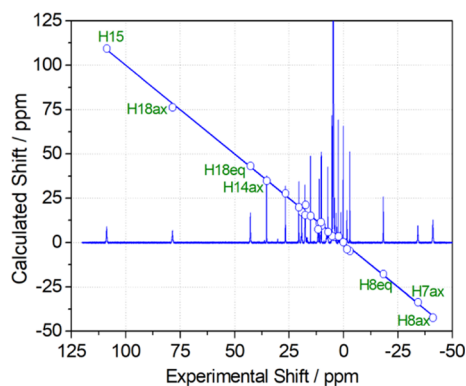


Figure 4. ¹H NMR spectrum of [Yb(CHXOCTAPA)]⁻ (300 MHz, 25 °C, pH 7.0) and plot of the calculated chemical shifts versus those obtained with eq 1 and the structure of the cis isomer. The line represents the identity line.

The spectrum was assigned on the basis of line-width analysis, as the paramagnetic contribution to the linewidths of ¹H resonances depends on $1/r^6$.⁷⁵ Thus, those protons located at shorter distances from the paramagnetic ion are characterized by broader resonances. Additional information for the assignment of the ¹H NMR spectrum was gained from ¹H,¹H-COSY measurements, which show cross-peaks relating the protons of the pyridyl units, the geminal CH₂ protons of the acetate and picolinate groups, and the protons of the cyclohexyl unit placed at a three-bond distance. The analysis of the paramagnetic shifts was accomplished by using eq 1, using the diamagnetic shifts observed for the Lu³⁺ analogue (Table S2, Supporting Information). Given the lack of any symmetry axis in the complex, the position of the magnetic axes cannot be anticipated. Thus, we performed a least squares fitting of the

paramagnetic shifts to eq 1 by using five fitting parameters: The axial ($\Delta\chi_{\text{ax}}/12\pi$) and rhombic ($\Delta\chi_{\text{rh}}/8\pi$) parts of the magnetic susceptibility tensor and three Euler angles relating the input orientation and that of the magnetic susceptibility tensor. The structure of the complex obtained with DFT calculations was used as a structural model.

The agreement of the chemical shifts observed for the Yb³⁺ complex and those calculated with eq 1 (and the estimates of the diamagnetic shifts using the Lu³⁺ complex) is excellent, with deviations <4.2 ppm and a mean deviation of 1.26 ppm (Figure 4, see also Table S2, Supporting Information). This is confirmed by the agreement factor $AF_i = 0.050$, which is similar to or better than those reported previously and considered to be satisfactory (0.06–0.11).^{76–80} Lower agreement factors were also calculated for symmetrical systems, but in those cases, the fit of the data involved a low number of experimental chemical shifts.⁷² This analysis indicates that the structure of the cis isomer obtained with DFT represents a good approximation of the actual structure of the complex in solution. Conversely, an unacceptable fit was obtained by using the trans isomer as the structural model ($AF_i = 0.363$), with deviations of the experimental and calculated data of up to ~34 ppm. As would be expected, the magnetic susceptibility tensor determined for the fit of the data for the cis isomer is rhombic, with $\Delta\chi_{\text{ax}}/12\pi = -2379 \pm 29$ ppm Å³ and $\Delta\chi_{\text{rh}}/8\pi = 919 \pm 65$ ppm Å³. The orientation of the magnetic axis is such that one of the picolinate lies close to the yz plane and one of the carboxylate groups on the xz plane (Figure S22, Supporting Information).

¹H NMRD and ¹⁷O NMR Studies. The relaxivity of [Gd(CHXOCTAPA)]⁻ was investigated in the proton Larmor frequency range 0.01–80 MHz, corresponding to magnetic field strengths varying between 2.34×10^{-4} and 1.88 T (Figure 5). The relaxivities recorded at 20 MHz (Table 3) are slightly higher than those reported for [Gd(OCTAPA)]⁻, [Gd(DOTA)]⁻, and [Gd(DTPA)]²⁻, but still consistent with the presence of a water molecule in the inner coordination sphere, as indicated by emission lifetime measurements (see above). As expected, fast rotation of the complex in solution limits proton relaxivity, which decreases with increasing temperature. Because the inner-sphere contribution to ¹H relaxivity is affected by a relatively large number of parameters, we have also recorded reduced longitudinal ($1/T_{1r}$) and transverse ($1/T_{2r}$) ¹⁷O NMR relaxation rates and reduced chemical shifts ($\Delta\omega_r$) of an aqueous solution of the complex (19.9 mM, pH = 7.27). These studies provide independent information about some important parameters that control ¹H relaxivity, especially the exchange rate of the coordinated water molecule(s) (k_{ex}^{298}) and the rotational correlation time (τ_R^{298}).⁸¹ The $1/T_{2r}$ values increase with decreasing temperature at high temperatures, reach a maximum at ca. 322 K, and then decrease. This is typical of systems that experience a changeover from a slow exchange regime at low temperature to a fast exchange condition at high temperature.⁸² The inflection point observed for the $1/T_{2r}$ values is also clearly visible in the chemical shift data.

A simultaneous fitting of the ¹H NMRD and ¹⁷O NMR data of [Gd(CHXOCTAPA)]⁻ was performed using a well-established methodology that treats the inner-sphere contribution to relaxivity with the Solomon–Bloembergen–Morgan theory^{83–85} and the outer-sphere mechanism with the translational diffusion model proposed by Freed.⁸⁶ The ¹⁷O NMR data were fitted with the standard Swift–

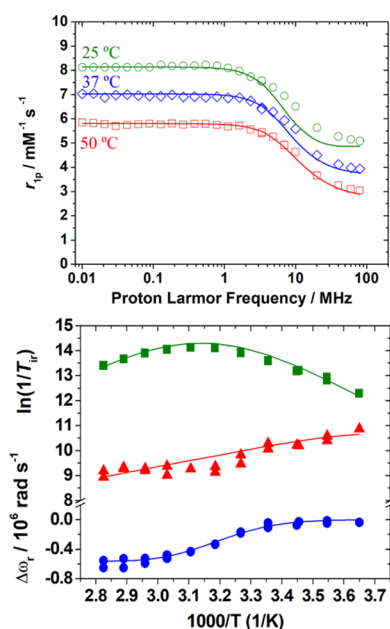


Figure 5. Top: ^1H NMRD profiles recorded at different temperatures for $[\text{Gd}(\text{CHXOCTAPA})]^-$ (pH 7.27). Bottom: Reduced transverse (green \blacksquare) and longitudinal (red \blacktriangle) ^{17}O NMR relaxation rates and ^{17}O NMR chemical shifts (blue \bullet) measured for $[\text{Gd}(\text{CHXOCTAPA})]^-$ at 9.4 T (0.0199 mM, pH = 7.27). The lines represent the fit of the data as explained in the text.

Connick^{87,88} equations. Several parameters have been fixed during the fitting procedure: the number of water molecules coordinated to the Gd^{3+} ion was fixed to $q = 1$ on the basis of the luminescence lifetime measurements described above, the distance of closest approach for the outer-sphere contribution a_{GdH} was fixed at 3.5 Å, and the distances between the Gd^{3+} ion and the H and O atoms of the coordinated water molecule (r_{GdH} and r_{GdO}) were set to the values obtained from DFT calculations. The value of the ^{17}O quadrupole coupling constant $\chi(1 + \eta^{2/3})^{1/2}$ was also estimated using DFT calculations. In previous studies, the quadrupole coupling constant was allowed to vary during the fitting procedure,⁸⁹ providing fitted values that deviated markedly from that

obtained for acidified water (7.58 MHz).⁹⁰ As a result, the fits of the data gave low rotational correlation times τ_{R} (Table 3). However, it has been demonstrated that coordination to Gd^{3+} provokes negligible changes in the quadrupole constant.⁹¹ Our calculations provided $\chi = 7.77$ MHz and an asymmetry parameter $\eta = 0.84$ ($\chi = 6.68$ MHz and $\eta = 0.93$ for pure water), yielding a $\chi(1 + \eta^{2/3})^{1/2}$ value of 10.7 MHz. Additional parameters that were fixed to reasonable values were the diffusion coefficient D_{GdH}^{298} ($20 \times 10^{-10} \text{ m}^2 \text{ s}^{-1}$), its activation energy E_{DGdH} (22 kJ mol^{-1}), and the activation energy for the modulation of the zero field splitting interaction ($E_{\text{v}} = 1 \text{ kJ mol}^{-1}$). The rotational correlation time τ_{R} affects both the T_1 ^{17}O relaxation rates and r_{lp} values. However, it has been shown that rotational correlation time characterizing the $\text{Ln}-\text{H}_{\text{water}}$ vector is $\sim 65\%$ shorter than that of the $\text{Ln}-\text{O}_{\text{water}}$ vector.⁹² Thus, we included in the fitting two different τ_{R} values with the constraint that $\tau_{\text{RH}}/\tau_{\text{RO}} = 0.65$.

An excellent fit of the ^{17}O NMR and ^1H NMRD data was obtained using the parameters listed in Table 3. The water exchange rate k_{ex}^{298} is lower than those determined for the complexes with OCTAPA^{4-} and DTPA^{5-} . A faster average exchange rate was also determined for the complexes with DOTA^{4-} , though in the latter case two isomers with very different water exchange parameters are present in solution.⁹³ The rigidity of the CHXOCTAPA^{4-} ligand likely increases the energy cost required to reach the transition state responsible for the water exchange process, resulting in a rather low water exchange rate.⁹⁴ A similar effect was observed previously upon rigidification of OCTAPA derivatives incorporating phosphonate groups.⁹⁵ The parameters characterizing the relaxation of the electron spin are very similar to those obtained for OCTAPA^{4-} , as would be expected from the similar relaxivities observed at low magnetic fields (<1 MHz). Complexes with DOTA^{4-} derivatives display slower electron spin relaxation, as a result of lower squared zero field splitting energies (Δ^2 , Table 3). Finally, the value obtained for the hyperfine coupling constant A/\hbar is in excellent agreement with that estimated with DFT ($3.10 \times 10^6 \text{ rad s}^{-1}$), which provides support to the reliability of the analysis.

Dissociation Kinetics. The slow dissociation of Ln^{3+} complexes is a key property for their application as both

Table 3. Parameters Obtained from the Simultaneous Analysis of ^{17}O NMR and ^1H NMRD Data

	CHXOCTAPA^{4-}	OCTAPA^{4-b}	DTPA^{5-c}	DOTA^{4-c}
r_{lp} at 25/37 °C, 20 MHz/mM $^{-1} \text{ s}^{-1}$	5.6/4.5	5.0/3.9	4.7/4.0	4.7/3.8
$k_{\text{ex}}^{298}/10^6 \text{ s}^{-1}$	1.58 ± 0.09	5.0	3.3	4.1
$\Delta H^\ddagger/\text{kJ mol}^{-1}$	54.6 ± 1.8	40.1	51.6	49.8
$\tau_{\text{RH}}^{298}/\text{ps}$	75 ± 3	55 ^b	58 ^b	77
$E_{\text{v}}/\text{kJ mol}^{-1}$	19.5 ± 1.2	17.9	17.3	16.1
$\tau_{\text{v}}^{298}/\text{ps}$	11.3 ± 0.06	12.6	25	11
$E_{\text{v}}/\text{kJ mol}^{-1}$	1.0 ^a	1.0 ^a	1.6	1.0 ^a
$\Delta^2/10^{20} \text{ s}^{-2}$	1.04 ± 0.06	1.2	0.46	0.16
$D_{\text{GdH}}^{298}/10^{-10} \text{ m}^2 \text{ s}^{-1}$	20.0 ^a	19	20	22
$E_{\text{DGdH}}/\text{kJ mol}^{-1}$	22 ^a	30.1	19.4	20.2
$A/\hbar/10^6 \text{ rad s}^{-1}$	-3.06 ± 0.08	-2.31	-3.8	-3.7
$\chi(1 + \eta^{2/3})^{1/2}/\text{MHz}$	10.7 ^a	17 ^b	14 ^b	10
$r_{\text{GdH}}/\text{Å}$	3.005 ^a	2.969 ^a	3.1 ^a	3.1 ^a
$r_{\text{GdO}}/\text{Å}$	2.480 ^a	2.54 ^a	2.5 ^a	2.5 ^a
$a_{\text{GdH}}/\text{Å}$	3.5 ^a	3.4 ^a	3.5 ^a	3.5 ^a
q^{298}	1 ^a	1 ^a	1 ^a	1 ^a

^aParameters fixed during the fitting procedure. ^bData from ref 26. ^cData from ref 89.

MRI contrast agents and radiopharmaceuticals. In the case of MRI contrast agents, there is an increasing concern on potential toxicity issues related to the release of Gd^{3+} in vivo.⁹⁶ Radiopharmaceuticals are injected in low doses, and thus chemical toxicity problems are likely not an important concern. However, complex dissociation may have negative effects by reducing the amount of radioisotope that reaches the desired target, thereby exposing to radiation healthy tissue.⁹⁷ In a previous paper, we analyzed the dissociation kinetics of the Gd^{3+} complex, which was found to be remarkably inert.³⁸ Herein, we present a detailed analysis of the dissociation kinetics of the Lu^{3+} analogue, given the potential of ^{177}Lu for therapeutic applications. We have shown recently that the dissociation kinetics of Ln^{3+} complexes may vary by several orders of magnitude across the lanthanide series, and thus the remarkable inertness of the Gd^{3+} complex does not necessarily ensure that the Lu^{3+} analogue behaves in a similar way.⁹⁸

The dissociation of the Lu^{3+} complex with CHXOCTAPA^{4-} was investigated by following the rates of exchange reactions taking place with Cu^{2+} at different proton concentrations (pH 3.30–4.72). The reactions were monitored in the presence of at least 10-fold Cu^{2+} excess to ensure pseudo first-order conditions. The observed rate constants display a rather unusual behavior, as increasing c_{H^+} provokes a slight initial decrease of the dissociation rates, which subsequently increase at higher c_{H^+} values. Furthermore, Cu^{2+} is also affecting significantly the complex dissociation rates (Figure 6). This

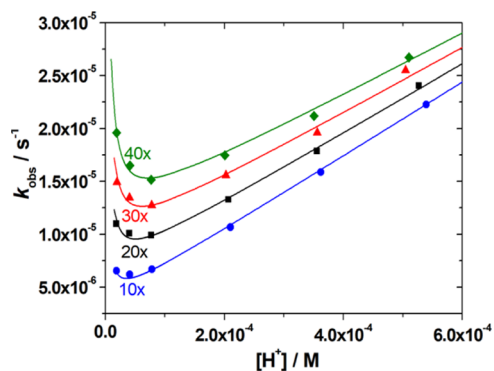


Figure 6. Plot of the pseudo-first-order rate constants measured for the $[\text{Lu}(\text{CHXOCTAPA})]^-$ as a function of H^+ ion concentration (50 mM DMP, 25 °C, 0.15 M NaCl) using different metal ion excess [10× (5.53 mM), 20× (11.07 mM), 30× (16.60 mM), and 40× (22.14 mM) was applied with pH = 3.30, 3.50, 3.80, 4.17, and 4.49]. The solid lines represent the fits of the data to eq 7.

indicates that the Lu^{3+} complex experiences dissociation by following the proton-assisted and metal-assisted pathways, the latter involving formation of a hetero-dinuclear complex. The dinuclear complex appears to form a hydroxo complex at relatively low pH that is responsible for the increase in k_{obs} values in the low proton concentration side (Figure 6). Thus, the dissociation of the complex can be expressed as in eq 2, where k_0 is the rate constant characterizing the spontaneous dissociation, k_{H} is the rate constant characterizing the proton-assisted dissociation, and k_{Cu} and $k_{\text{Cu}}^{\text{OH}}$ are associated with the metal-assisted dissociation pathways, the latter with the formation of a hydroxo dinuclear complex.

$$-\frac{d[\text{Lu}(\text{L})]_t}{dt} = k_{\text{obs}}[\text{Lu}(\text{L})]_t \\ = k_0[\text{Lu}(\text{L})] + k_{\text{H}}[\text{Lu}(\text{HL})] \\ + k_{\text{Cu}}[\text{Lu}(\text{L})\text{Cu}] + k_{\text{Cu}}^{\text{OH}}[\text{Lu}(\text{L})\text{Cu}(\text{OH})] \quad (2)$$

Considering that the total concentration of complexed Lu^{3+} is given by eq 3 and the equilibrium constants defined by eqs 4–6, the rate constants can be expressed as in eq 7, where $k_1 = k_{\text{H}} \times K_{\text{H}}$, $k_3^{\text{Cu}} = k_{\text{Cu}}K_{\text{Cu}}$, and $k_6^{\text{Cu}} = k_{\text{Cu}}^{\text{OH}}K_{\text{Cu}}K_{\text{Cu}}^{\text{OH}}$.

$$[\text{Lu}(\text{L})]_t = [\text{LuL}] + [\text{Lu}(\text{HL})] + [\text{Lu}(\text{L})\text{M}] \\ + [\text{Lu}(\text{L})\text{MOH}] \quad (3)$$

$$K_{\text{H}} = \frac{[\text{Lu}(\text{HL})]}{[\text{LuL}][\text{H}^+]} \quad (4)$$

$$K_{\text{Cu}} = \frac{[\text{Lu}(\text{L})\text{Cu}]}{[\text{Lu}(\text{L})][\text{Cu}^{2+}]} \quad (5)$$

$$K_{\text{CuOH}} = \frac{[\text{Lu}(\text{L})\text{Cu}(\text{OH})]K_{\text{w}}}{[\text{Lu}(\text{L})\text{Cu}][\text{H}^+]} \quad (6)$$

$$k_{\text{obs}} = \frac{k_0 + k_1[\text{H}^+] + k_3[\text{Cu}^{2+}] + k_6[\text{Cu}^{2+}]K_{\text{w}}/[\text{H}^+]}{1 + K_{\text{H}}[\text{H}^+] + K_{\text{Cu}}[\text{Cu}^{2+}] + K_{\text{Cu}(\text{OH})}K_{\text{Cu}}[\text{Cu}^{2+}]K_{\text{w}}/[\text{H}^+]} \quad (7)$$

Attempts to fit the data to eq 7 including k_0 as fitting parameter provided a small negative value, which indicates that spontaneous dissociation does not play any role under the conditions used for kinetic experiments. Furthermore, it is difficult to estimate the rate constant characterizing the spontaneous reaction pathway within the same pH range where the dissociation of the $\text{Lu}(\text{L})\text{Cu}(\text{OH})$ complex takes

Table 4. Rate and Equilibrium Constants Characterizing the Dissociation of the CHXOCTAPA^{4-} Complexes and Related Systems (25 °C)

	$[\text{LuCHXOCTAPA}]^-$	$[\text{GdCHXOCTAPA}]^-$ ^a	$[\text{GdOCTAPA}]^-$ ^b	$[\text{GdDTPA}]2^-$ ^c	$[\text{GdDO3A}]^d$
$k_1/\text{M}^{-1} \text{s}^{-1}$	$3.74 \pm 0.06 \times 10^{-2}$	1.60×10^{-2}	11.8	0.58	0.023
$k_2/\text{M}^{-2} \text{s}^{-2}$			2.5×10^4	9.7×10^4	
$k_3^{\text{Cu}}/\text{M}^{-1} \text{s}^{-1}$	$6.3 \pm 0.3 \times 10^{-4}$	6.8×10^{-4}	22.5	0.93	
$k_6^{\text{Cu}}/\text{M}^{-2} \text{s}^{-1}$	$5.1 \pm 0.3 \times 10^5$		5.0×10^9		
K_{H}		737	2.6	100	
K_{Cu}	12.1 ± 1.6	48		13	
$t_{1/2}/\text{h}^e$	876	1.49×10^5	0.15	202	2.10×10^5

^aData from ref 38. ^bData from ref 26. ^cData from ref 25. ^dData from ref 47. ^eHalf-lives determined at pH 7.4 and $[\text{Cu}^{2+}] = 1 \mu\text{M}$.

place, as the latter acts as a competitive dissociation path to the spontaneous dissociation. A similar situation occurred for K_{H} , revealing that the $K_{\text{H}}[\text{H}^+]$ term in the denominator of eq 7 has a negligible contribution to k_{obs} . This is expected considering the low protonation constants determined using potentiometry ($\log K_{\text{LnH}}$ in the range 1–2, Table 1) and the relatively low proton concentrations used for kinetic experiments ($<10^{-6}$ M, Figure 6). The results of the fit are shown in Table 4, together with a comparison with the data reported previously for the Gd^{3+} complexes of CHXOCTAPA^{4-} ,³⁸ OCTAPA^{4-} ,³¹ DTPA^{5-} ,²⁵ and DO3A^{3-} .⁴⁷ It is worth mentioning that the dissociation pathway through formation of a hydroxo dinuclear species was not detected for the Gd^{3+} analogue, which was investigated in approximately the same pH range. The formation of hydroxo complexes is more likely to occur as the size of the lanthanide ion decreases across the series due to the lanthanide contraction, as indicated by the corresponding hydrolysis constants ($\log K_{\text{Ln(OH)}} = -7.83$ and -7.27 for Gd^{3+} and Lu^{3+} , respectively).⁹⁹ Alternatively, the structural change occurring close to the center of the lanthanide series could be responsible for the different behavior of the Gd^{3+} and Lu^{3+} complexes.

The rate constants shown in Table 4 indicate that the Gd^{3+} and Lu^{3+} analogues present similar inertness with respect to their dissociation following the proton-assisted and metal-assisted pathways, as judged by the values of the k_1 and k_3^{Cu} rate constants. However, the metal-assisted pathway with the formation of a hydroxo complex, characterized by k_6^{Cu} , plays an increasingly important role in the dissociation of the complex as the concentration of OH^- increases. As a result, this pathway is mainly responsible for complex dissociation at pH 7.4, a situation that is clearly reflected in the half-lives of the complex calculated at pH 7.4 using $[\text{Cu}^{2+}] = 1 \mu\text{M}$ (Table 4). Nevertheless, the half-life estimated for $[\text{Lu}(\text{CHXOCTAPA})]^-$ remains three times longer than that of $[\text{Gd}(\text{DTPA})]^{2-}$, but clearly shorter than that of the macrocyclic complex $[\text{Gd}(\text{DO3A})]$. The effect that the rigid cyclohexyl unit has in improving kinetic inertness is also obvious when comparing the half-lives of CHXOCTAPA^{4-} and OCTAPA^{4-} derivatives.

CONCLUSIONS

The present contribution has shown that the octadentate CHXOCTAPA^{4-} ligand forms fairly stable complexes with the Ln^{3+} ions, with stability constants in the range $\log K_{\text{LnL}} \sim 17.8$ – 19.7 . The presence of the rigid cyclohexyl ring causes a slight increase of the selectivity of the ligand for the Ln^{3+} ions over Cu^{2+} and Zn^{2+} . The picolinate units are rather efficient in sensitizing the Eu^{3+} and particularly Tb^{3+} luminescence, with emission quantum yields comparable to those of the OCTAPA^{4-} analogues. The complexes are monohydrated ($q = 1$) in solution, as indicated by emission lifetime measurements. The exchange rate of the water molecule coordinated to Gd^{3+} (as confirmed by ^{17}O NMR studies) is rather low when compared with the OCTAPA^{4-} , DTPA^{5-} , and DOTA^{4-} analogues, likely as a result of the rigid structure of the complex.

The coordination chemistry reported in this paper provided two unexpected results. First, the analysis of the structural information encoded by the pseudocontact shifts, induced by Yb^{3+} , demonstrate that this complex presents an unusual cis structure in which the amine N atoms adopt *S,R* configurations. DFT calculations show that this conformation is

stabilized across the lanthanide series over the *trans R,R* (or *S,S*) conformation. The presence of the cyclohexyl group causes a significant stabilization of the *S,R* conformation. A second unexpected effect was observed when investigating the dissociation of the Lu^{3+} complex in the presence of exchanging Cu^{2+} ions. Complex dissociation at physiological pH was found to occur mainly through the metal-assisted mechanism that involves the formation of a hydroxo complex, a pathway that was not observed previously for the Gd^{3+} analogue. We hypothesize that this pathway may be relevant for the dissociation of complexes of acidic cations relevant for radiopharmaceutical applications (i.e., Sc^{3+}).

EXPERIMENTAL AND COMPUTATIONAL SECTION

Materials. The $\text{H}_4\text{CHXOCTAPA}$ and H_4OCTAPA ligands were prepared as described in previous papers.^{31,38} All other chemicals and solvents were purchased from commercial sources and used without further purification. The complexes used for NMR and photophysical studies were prepared by mixing stoichiometric amounts of the ligand and the corresponding $\text{Ln}(\text{OTf})_3$ salts and subsequent adjustment of the pH with diluted NaOH/NaOD solutions.

NMR Spectroscopy. ^1H NMR spectra were recorded at 25 °C in solutions of the complexes in D_2O using Bruker Avance 300 or Bruker ARX400 spectrometers. Chemical shifts were referenced by using the residual solvent HDO proton signal ($\delta = 4.79$ ppm).¹⁰⁰

The ^1H NMRD measurements were carried out by using a Stelar SMARTracer Fast Field Cycling relaxometer (0.01–10 MHz) and a Bruker WP80 NMR electromagnet adapted to variable field measurements (20–80 MHz) controlled by a SMARTracer PC-NMR console. The NMRD profiles of the $[\text{Gd}(\text{CHXOCTAPA})]^-$ complex ($c_{\text{complex}} = 2.69$ mM) were recorded in aqueous solution at three different temperatures (25, 37 and 50 °C) in the presence of 4-(2-hydroxyethyl)-1-piperazineethanesulfonic acid buffer (25 mM, pH = 7.27) to maintain the pH constant. The temperature of the samples was managed by a VTC91 temperature control unit (calibrated by a Pt resistance temperature probe) and maintained by gas flow.

Transverse and longitudinal ^{17}O relaxation rates ($1/T_2$, $1/T_1$) and chemical shifts were measured in aqueous solutions of $[\text{Gd}(\text{CHXOCTAPA})]^-$ (0.0199 mM, pH = 7.27) in the temperature range 274–354 K on a Bruker Avance 400 (9.4 T, 54.24 MHz) spectrometer. The temperature was calculated according to previous calibration with ethylene glycol and methanol.¹⁰¹ An acidified water solution (HClO_4 , pH 3.3) was used as an external reference. Longitudinal relaxation times (T_1) were obtained by the inversion–recovery method, and transverse relaxation times (T_2) were obtained by the Carr–Purcell–Meiboom–Gill spin-echo technique.¹⁰² The technique used for ^{17}O NMR measurements on Gd^{3+} complexes has been described elsewhere.¹⁰³ The samples were sealed in glass spheres fitted into 10 mm NMR tubes to avoid susceptibility corrections of the chemical shifts.¹⁰⁴ To improve the sensitivity, ^{17}O -enriched water (10% H_2^{17}O , CortecNet) was added to the solutions to reach around 2% enrichment. The ^{17}O NMR data were treated according to the Solomon–Bloembergen–Morgan theory of paramagnetic relaxation. The least-squares fit of the ^{17}O NMR and ^1H NMRD data was performed using Micromath Scientist version 2.0 (Salt Lake City, UT, USA).

Absorption and Emission Electronic Spectroscopy. The absorption spectra of the Eu^{3+} and Tb^{3+} complexes were recorded with a Jasco V-650 spectrometer using 0.2 cm quartz cells. Steady-state emission spectra were obtained with a Horiba FluoroMax Plus-P spectrofluorometer using a 150 W ozone-free xenon arc lamp as the excitation source, a R928P photon counting emission detector, and an integration time of 0.1 s. Luminescence lifetimes were measured using the time-correlated single photon counting technique and a pulsed xenon flash lamp as the excitation source. Quantum yields were determined using the $\text{Cs}_3[\text{Ln}(\text{pic})_3]$ complexes (pic = 2,6-dipicolinate, Ln = Eu or Tb) as standards ($\Phi_{\text{Eu}} = 24\%$ in TRIS, pH 7.4, 7.5×10^{-5} M; $\Phi_{\text{Tb}} = 22\%$ in TRIS, pH 7.4, 6.5×10^{-5} M).^{52,53}

Equilibrium Studies. The chemicals (MCl_2 and LnCl_3 salts) used in the studies were of the highest analytical grade obtained from commercial sources (Sigma-Aldrich and Strem Chemicals Inc.). The concentration of the stock solutions was determined by complexometric titration using a standardized $\text{Na}_2\text{H}_2\text{EDTA}$ solution and appropriate indicators (Patton & Reeder (CaCl_2), Eriochrome Black T (MgCl_2), xylenol orange (ZnCl_2 and LnCl_3), and murexide (CuCl_2)).

The pH potentiometric titrations were carried out with a Metrohm 888 Titrandro titration workstation using a Metrohm-6.0233.100 combined electrode. The titrated solutions (6.00 mL) were thermostated at 25 °C, and samples were stirred and kept under an inert gas atmosphere (N_2) to avoid the presence of CO_2 . The calibration of the electrode was performed by a two-point calibration [KH-phthalate (pH = 4.005) and borax (pH = 9.177) buffers] routine. The calculation of $[\text{H}^+]$ from the measured pH values was performed with the use of the method proposed by Irving et al.¹⁰⁵ by titrating a 0.01 M HCl solution ($I = 0.15$ M NaCl) with a standardized NaOH solution. The differences between the measured (pH_{read}) and calculated pH ($-\log [\text{H}^+]$) values were used to obtain the equilibrium H^+ concentrations from the pH data obtained in the titrations. The ion product of water ($\text{p}K_{\text{w}} = 13.847$) was determined from the same experiment in the pH range 11.2–11.85.

The concentration of the CHXOCTAPA^{4-} chelator was determined by pH potentiometric titration, comparing the titration curves obtained in the presence and absence of high Ca^{2+} excess (the concentration of the ligand in the titration was 4.38 mM). The protonation constants of CHXOCTAPA^{4-} , the stability and protonation constants of the complexes formed with Mg^{2+} , Ca^{2+} , Cu^{2+} and Zn^{2+} , as well as those of La^{3+} , Gd^{3+} , and Yb^{3+} were also determined by pH potentiometric titration. The metal-to-ligand concentration ratios were 1:1 and 2:1 (the concentration of the ligand in these titrations was generally 2.50–3.00 mM). The pH potentiometric titration curves were measured in the pH range 1.70–11.85, while 122–356 mL NaOH-pH data pairs were recorded and fitted simultaneously.

Due to the high conditional stability of $[\text{Cu}(\text{CHXOCTAPA})]^{2-}$, the formation of the complex was complete (nearly 100%) even at pH = 1.75 (starting point of the pH potentiometric titrations). For this reason, 12 out-of-cell (batch) samples containing a slight excess of ligand and the Cu^{2+} ion were prepared ($[\text{L}] = 3.110$ mM, $[\text{Cu}^{2+}] = 3.065$ mM, 25 °C, 3.0 M ($\text{Na}^+ + \text{H}^+$) Cl^-). The samples, whose acidity was varied in the concentration range of 0.1005–3.007 M, were equilibrated for 1 day before recording the absorption spectra at 25 °C in Peltier thermostated semimicro 1 cm Hellma cells using a Jasco V-770 UV–vis–NIR spectrophotometer. The molar absorptivity of the $[\text{Cu}(\text{CHXOCTAPA})]^{2-}$ complex was determined at 25 wavelengths (600–840 nm range) by recording the spectra of 1.501×10^{-3} , 3.002×10^{-3} , and 4.503×10^{-3} M solutions of the complex, while for the Cu^{2+} ion, previously published molar absorptivity values (determined under identical conditions) were used for data fitting.¹⁰⁶ The molar absorption coefficients of the protonated $[\text{CuH}(\text{CHXOCTAPA})]^-$ and $[\text{CuH}_2(\text{CHXOCTAPA})]$ species were calculated during data refinement (UV–visible and pH potentiometric titration curves obtained at various metal to ligand concentrations were fitted simultaneously). The protonation (ligand and complexes) and stability constants (complexes) were calculated from the titration data with the PSEQUAD program.¹⁰⁷

Stability constants of the $[\text{Zn}(\text{CHXOCTAPA})]^{2-}$, $[\text{La}(\text{CHXOCTAPA})]^-$, and $[\text{Yb}(\text{CHXOCTAPA})]^-$ complexes were also determined by following the competition reaction of these metal ions with Gd^{3+} for the ligand, in a similar manner as it was performed for the $[\text{M}(\text{OCTAPA})]^{4-}$ complexes.³¹ A total of 9–11 samples containing nearly 1 mM $[\text{Gd}(\text{CHXOCTAPA})]^-$ and 0.5–20.0 mM (La^{3+}), 0.25–35.0 mM (Yb^{3+}), or 0.5–20 mM (Zn^{2+}) metal chlorides were prepared and equilibrated at constant pH (4.69 for La^{3+} , 4.79 for Yb^{3+} , and 4.81 for Zn^{2+}). Longitudinal relaxation times of the samples were measured after 4 weeks (and repeated 4 weeks later to make sure that the equilibrium had been reached) and the formation constants determined by using the relaxivities of the Gd^{3+}

aqua ion and $[\text{Gd}(\text{CHXOCTAPA})]^-$ (13.26 and 6.16 $\text{mM}^{-1} \text{s}^{-1}$ at 25 °C and 0.49 T, respectively).³⁸

Kinetic Studies. The rates of the metal exchange reactions involving the $[\text{Lu}(\text{CHXOCTAPA})]^-$ complex and Cu^{2+} were studied by using UV–vis spectrophotometry following the formation of the $[\text{Cu}_2(\text{CHXOCTAPA})]$ complex. The conventional UV–vis spectroscopic method was applied to follow the decomplexation reactions of $[\text{Lu}(\text{CHXOCTAPA})]^-$, as these reactions were very slow even at relatively low pH (in the pH range 3.27–4.39). The absorbance versus time kinetic curves were acquired by using a Jasco V-770 UV–vis–NIR spectrophotometer equipped with Peltier thermostatted multicell holder. The temperature was maintained at 25 °C, and the ionic strength of the solutions was kept constant by using 0.15 M NaCl. For keeping the pH constant, 50 mM DMP buffer was used ($\log K_2^{\text{H}} = 4.19(5)$ as determined by using pH-potentiometry at 25 °C with the use of 0.15 M NaCl ionic strength). The exchange reactions were followed continuously at 300 nm for 4–5 days (80–95% conversion) and occasionally (one or two readouts per day) for another 5–7 days. The absorbance readings at equilibrium were determined 3–4 weeks after the start of the reaction depending on the pH of the samples (8–10 times longer than the half-life of the reaction). The concentration of the $[\text{Lu}(\text{CHXOCTAPA})]^-$ chelate was 0.52 mM, while the Cu^{2+} ion was applied at high excess (10.6–42.6 fold) in order to ensure pseudo-first order conditions. The pseudo-first-order rate constants (k_{obs}) were calculated by fitting the absorbance–time data pairs to eq 8

$$A_t = (A_0 - A_e)e^{-k_{\text{obs}}t} + A_e \quad (8)$$

where A_t , A_0 , and A_e are the absorbance at time t , at the start, and at equilibrium, respectively. The pseudo-first-order rate constants were fitted with the computer program Micromath Scientist, version 2.0 (Salt Lake City, UT, USA) by using a standard least-squares procedure.

Computational Studies. The geometries of the $[\text{Ln}(\text{OCTAPA})(\text{H}_2\text{O})]^{2-} \cdot 2\text{H}_2\text{O}$ and $[\text{Ln}(\text{CHXOCTAPA})(\text{H}_2\text{O})]^{2-} \cdot 2\text{H}_2\text{O}$ systems ($\text{Ln} = \text{La}, \text{Pr}, \text{Gd}, \text{Yb}, \text{or Lu}$) were optimized using DFT calculations with the M062X¹⁰⁸ exchange correlation functional. Two explicit second-sphere water molecules were considered in these models for a more appropriate description of the interaction between the metal ion and the coordinated water molecule.¹⁰⁹ Relativistic effects were considered with the pseudopotential approximation using either the large-core quasi-relativistic effective core potentials (ECP) developed by Dolg et al. ($[\text{Kr}4d^{10}4f^m \text{ core}]^{110}$ and the $(14s6p5d)/[2s1p1d]$ -GTO valence basis sets ($\text{Ln} = \text{Pr}, \text{Gd}, \text{Yb}$ and Lu) or the small-core quasi-relativistic ECP ($1s$ – $3d$ electrons in the core)¹¹¹ and the associated $(42s26p20d8f)/[3s2p2d1f]$ valence basis set ($\text{Ln} = \text{La}$). All other atoms were described using the standard 6-311G(d,p) basis set. Bulk solvent effects were incorporated using the integral equation formalism implementation of the polarized continuum model.¹¹² Frequency calculations were performed to confirm that geometry optimizations provided local energy minima on the corresponding potential energy surfaces. All pseudopotential calculations were carried out with the Gaussian 16 program.¹¹³

Hyperfine and quadrupole coupling constants¹¹⁴ of the O atoms of water molecules coordinated to Gd^{3+} were estimated with DFT using the ORCA4 program package^{115,116} and a Gaussian finite model.¹¹⁷ In these calculations, we used the hybrid *meta*-GGA TPSSH functional,¹¹⁸ which was found to provide good estimates of hyperfine coupling constants in Gd^{3+} ^{109,119} and other metal complexes.¹²⁰ Relativistic effects were introduced with the Douglas–Kroll–Hess (DKH2) method,^{121,122} using the SARC2-DKH-QZVP¹²³ for Gd and the DKH-def2-TZVPP¹²⁴ basis set for all other atoms. The resolution of identity and chain of spheres^{125,126} algorithm was used to speed up the calculation with the aid of auxiliary basis sets generated with the Autoaux¹²⁷ procedure for Gd and the SARC/J auxiliary basis set for all other atoms (decontracted Def2/J).¹²⁸ Bulk solvent effects were considered with the SMD solvation model developed by Truhlar.¹²⁹

■ ASSOCIATED CONTENT

SI Supporting Information

The Supporting Information is available free of charge at <https://pubs.acs.org/doi/10.1021/acs.inorgchem.2c00501>.

Absorption and emission spectra, NMR spectra, speciation diagrams, analysis of the Yb³⁺-induced paramagnetic shifts, bond distances, and optimized geometries obtained with DFT (PDF)

■ AUTHOR INFORMATION

Corresponding Authors

Gyula Tircsó – Department of Physical Chemistry, University of Debrecen, H-4010 Debrecen, Hungary; orcid.org/0000-0002-7896-7890; Email: gyula.tircso@science.unideb.hu

Carlos Platas-Iglesias – Centro de Investigaciones Científicas Avanzadas (CICA) and Departamento de Química, Facultade de Ciencias, Universidade da Coruña, 15071 A Coruña, Spain; orcid.org/0000-0002-6989-9654; Email: carlos.platas.iglesias@udc.es

Authors

Fátima Lucio-Martínez – Centro de Investigaciones Científicas Avanzadas (CICA) and Departamento de Química, Facultade de Ciencias, Universidade da Coruña, 15071 A Coruña, Spain; orcid.org/0000-0002-4505-2360

Zoltán Garda – Department of Physical Chemistry, University of Debrecen, H-4010 Debrecen, Hungary

Balázs Váradi – Department of Physical Chemistry and Doctoral School of Chemistry, University of Debrecen, H-4010 Debrecen, Hungary

Ferenc Krisztián Kálmán – Department of Physical Chemistry, University of Debrecen, H-4010 Debrecen, Hungary; orcid.org/0000-0001-9000-2779

David Esteban-Gómez – Centro de Investigaciones Científicas Avanzadas (CICA) and Departamento de Química, Facultade de Ciencias, Universidade da Coruña, 15071 A Coruña, Spain

Éva Tóth – Centre de Biophysique Moléculaire, CNRS UPR 4301, Université d'Orléans, 45071 Orléans, France

Complete contact information is available at: <https://pubs.acs.org/doi/10.1021/acs.inorgchem.2c00501>

Notes

The authors declare no competing financial interest.

■ ACKNOWLEDGMENTS

F.L.-M., D.E.-G., and C.P.-I. thank Ministerio de Ciencia e Innovación (Grant PID2019-104626GB-I00) and Xunta de Galicia (ED431B 2020/52) for generous financial support. The authors thank the financial support for the Hungarian National Research, Development and Innovation Office (NKFIH K-128201, 134694 and FK-134551 projects). G.T. and C.P.-I. gratefully acknowledge the bilateral Hungarian–Spanish Science and Technology Cooperation Program (2019-2.1.11-TET-2019-00084 supported by NKFIH). B.V. was supported by the Doctoral School of Chemistry at the University of Debrecen, Debrecen, Hungary. This publication and the scientific research were supported by the Gedeon Richter's Talentum Foundation established by Gedeon Richter Plc (Gedeon Richter Ph.D. Fellowship). The research was prepared with the professional support of the Doctoral Student

Scholarship Program of the Cooperative Doctoral Program of the Ministry of Innovation and Technology financed from the National Research, Development and Innovation Fund (NKFIH). The research was supported by the ÚNKP-21-4 new national excellence program of the Ministry of Human Capacities (F.K.K.) and the János Bolyai Research Scholarship of the Hungarian Academy of Sciences (F.K.K.). The authors are indebted to Centro de Supercomputación de Galicia (CESGA) for providing the computer facilities. C.P.-I. thanks Prof. M. Mazzanti for noticing that the emission quantum yields reported previously for OCTAPA⁴⁺ complexes were incorrect. Funding for open access provided by Universidade da Coruña/CISUG.

■ REFERENCES

- (1) Wahsner, J.; Gale, E. M.; Rodríguez-Rodríguez, A.; Caravan, P. Chemistry of MRI Contrast Agents: Current Challenges and New Frontiers. *Chem. Rev.* **2019**, *119*, 957–1057.
- (2) Heffern, M. C.; Matosziuk, L. M.; Meade, T. J. Lanthanide Probes for Bioresponsive Imaging. *Chem. Rev.* **2014**, *114*, 4496–4539.
- (3) Li, H.; Meade, T. J. Molecular Magnetic Resonance Imaging with Gd(III)-Based Contrast Agents: Challenges and Key Advances. *J. Am. Chem. Soc.* **2019**, *141*, 17025–17041.
- (4) Pierre, V. C.; Harris, S. M.; Pailloux, S. L. Comparing Strategies in the Design of Responsive Contrast Agents for Magnetic Resonance Imaging: A Case Study with Copper and Zinc. *Acc. Chem. Res.* **2018**, *51*, 342–351.
- (5) Angelovski, G.; Tóth, É. Strategies for Sensing Neurotransmitters with Responsive MRI Contrast Agents. *Chem. Soc. Rev.* **2017**, *46*, 324–336.
- (6) Bünzli, J.-C. G. Lanthanide Luminescence for Biomedical Analyses and Imaging. *Chem. Rev.* **2010**, *110*, 2729–2755.
- (7) Bünzli, J.-C. G. On the Design of Highly Luminescent Lanthanide Complexes. *Coord. Chem. Rev.* **2015**, *293–294*, 19–47.
- (8) Nonat, A. M.; Charbonnière, L. J. Upconversion of Light with Molecular and Supramolecular Lanthanide Complexes. *Coord. Chem. Rev.* **2020**, *409*, 213192.
- (9) Kostelnik, T. I.; Orvig, C. Radioactive Main Group and Rare Earth Metals for Imaging and Therapy. *Chem. Rev.* **2019**, *119*, 902–956.
- (10) Vaughn, B. A.; Koller, A. J.; Chen, Z.; Ahn, S. H.; Loveless, C. S.; Cingoranelli, S. J.; Yang, Y.; Cirri, A.; Johnson, C. J.; Lapi, S. E.; Chapman, K. W.; Boros, E. Homologous Structural, Chemical, and Biological Behavior of Sc and Lu Complexes of the Picagat Bifunctional Chelator: Toward Development of Matched Theranostic Pairs for Radiopharmaceutical Applications. *Bioconjugate Chem.* **2021**, *32*, 1232–1241.
- (11) Baranyai, Z.; Pálkás, Z.; Uggeri, F.; Maiocchi, A.; Aime, S.; Brücher, E. Dissociation Kinetics of Open-Chain and Macrocyclic Gadolinium(III)-Aminopolycarboxylate Complexes Related to Magnetic Resonance Imaging: Catalytic Effect of Endogenous Ligands. *Chem.—Eur. J.* **2012**, *18*, 16426–16435.
- (12) Baranyai, Z.; Brücher, E.; Uggeri, F.; Maiocchi, A.; Tóth, I.; András, M.; Gáspár, A.; Zékány, L.; Aime, S. The Role of Equilibrium and Kinetic Properties in the Dissociation of Gd[DTPA-Bis-(Methylamide)] (Omniscan) at near to Physiological Conditions. *Chem.—Eur. J.* **2015**, *21*, 4789–4799.
- (13) Boros, E.; Packard, A. B. Radioactive Transition Metals for Imaging and Therapy. *Chem. Rev.* **2019**, *119*, 870–901.
- (14) Shuvaev, S.; Starck, M.; Parker, D. Responsive, Water-Soluble Europium(III) Luminescent Probes. *Chem.—Eur. J.* **2017**, *23*, 9974–9989.
- (15) Clough, T. J.; Jiang, L.; Wong, K.-L.; Long, N. J. Ligand Design Strategies to Increase Stability of Gadolinium-Based Magnetic Resonance Imaging Contrast Agents. *Nat. Commun.* **2019**, *10*, 1420.

- (16) Hermann, P.; Kotek, J.; Kubíček, V.; Lukeš, I. Gadolinium(III) Complexes as MRI Contrast Agents: Ligand Design and Properties of the Complexes. *Dalton Trans.* **2008**, 23, 3027–3047.
- (17) Baranyai, Z.; Uggeri, F.; Giovenzana, G. B.; Bényei, A.; Brücher, E.; Aime, S. Equilibrium and Kinetic Properties of the Lanthanoids(III) and Various Divalent Metal Complexes of the Heptadentate Ligand AAZTA. *Chem.—Eur. J.* **2009**, 15, 1696–1705.
- (18) Gritmon, T. F.; Goedken, M. P.; Choppin, G. R. The Complexation of Lanthanides by Aminocarboxylate Ligands—I. *J. Inorg. Nucl. Chem.* **1977**, 39, 2021–2023.
- (19) Tei, L.; Baranyai, Z.; Brücher, E.; Cassino, C.; Demicheli, F.; Masciocchi, N.; Giovenzana, G. B.; Botta, M. Dramatic Increase of Selectivity for Heavy Lanthanide(III) Cations by Tuning the Flexibility of Polydentate Chelators. *Inorg. Chem.* **2010**, 49, 616–625.
- (20) Baranyai, Z.; Pálkás, Z.; Uggeri, F.; Brücher, E. Equilibrium Studies on the Gd^{3+} , Cu^{2+} and Zn^{2+} Complexes of BOPTA, DTPA and DTPA-BMA Ligands: Kinetics of Metal-Exchange Reactions of $[Gd(BOPTA)]^{2+}$. *Eur. J. Inorg. Chem.* **2010**, 1948–1956.
- (21) Rodríguez-Rodríguez, A.; Esteban-Gómez, D.; Tripier, R.; Tircsó, G.; Garda, Z.; Tóth, I.; de Blas, A.; Rodríguez-Blas, T.; Platas-Iglesias, C. Lanthanide(III) Complexes with a Reinforced Cyclam Ligand Show Unprecedented Kinetic Inertness. *J. Am. Chem. Soc.* **2014**, 136, 17954–17957.
- (22) Balogh, E.; Tripier, R.; Ruloff, R.; Tóth, É. Kinetics of Formation and Dissociation of Lanthanide(III) Complexes with the 13-Membered Macrocyclic Ligand TRITA⁴⁻. *Dalton Trans.* **2005**, 6, 1058–1065.
- (23) Toth, E.; Brucher, E.; Lazar, I.; Toth, I. Kinetics of Formation and Dissociation of Lanthanide(III)-DOTA Complexes. *Inorg. Chem.* **1994**, 33, 4070–4076.
- (24) Wu, S. L.; Horrocks, W. D. Kinetics of Complex Formation by Macrocyclic Polyaza Polycarboxylate Ligands: Detection and Characterization of an Intermediate in the Eu^{3+} -Dota System by Laser-Excited Luminescence. *Inorg. Chem.* **1995**, 34, 3724–3732.
- (25) Sarka, L.; Burai, L.; Brücher, E. The Rates of the Exchange Reactions between $[Gd(DTPA)]^{2+}$ and the Endogenous Ions Cu^{2+} and Zn^{2+} : A Kinetic Model for the Prediction of the In Vivo Stability of $[Gd(DTPA)]^{2+}$, Used as a Contrast Agent in Magnetic Resonance Imaging. *Chem.—Eur. J.* **2000**, 6, 719–724.
- (26) Platas-Iglesias, C.; Mato-Iglesias, M.; Djanashvili, K.; Muller, R. N.; Elst, L. V.; Peters, J. A.; de Blas, A.; Rodríguez-Blas, T. Lanthanide Chelates Containing Pyridine Units with Potential Application as Contrast Agents in Magnetic Resonance Imaging. *Chem.—Eur. J.* **2004**, 10, 3579–3590.
- (27) Chatterton, N.; Gateau, C.; Mazzanti, M.; Pécaut, J.; Borel, A.; Helm, L.; Merbach, A. The Effect of Pyridinecarboxylate Chelating Groups on the Stability and Electronic Relaxation of Gadolinium Complexes. *Dalton Trans.* **2005**, 6, 1129–1135.
- (28) Borel, A.; Laus, S.; Ozarowski, A.; Gateau, C.; Nonat, A.; Mazzanti, M.; Helm, L. Multiple-Frequency EPR Spectra of Two Aqueous Gd^{3+} Polyamino Polypyridine Carboxylate Complexes: A Study of High Field Effects. *J. Phys. Chem. A* **2007**, 111, 5399–5407.
- (29) Jaraquemada-Peláez, M. d. G.; Wang, X.; Clough, T. J.; Cao, Y.; Choudhary, N.; Emler, K.; Patrick, B. O.; Orvig, C. H_4 Octapa: Synthesis, Solution Equilibria and Complexes with Useful Radiopharmaceutical Metal Ions. *Dalton Trans.* **2017**, 46, 14647–14658.
- (30) Price, E. W.; Cawthray, J. F.; Bailey, G. A.; Ferreira, C. L.; Boros, E.; Adam, M. J.; Orvig, C. H_4 Octapa: An Acyclic Chelator for ^{111}In Radiopharmaceuticals. *J. Am. Chem. Soc.* **2012**, 134, 8670–8683.
- (31) Kálmán, F. K.; Végh, A.; Regueiro-Figueroa, M.; Tóth, É.; Platas-Iglesias, C.; Tircsó, G. H_4 Octapa: Highly Stable Complexation of Lanthanide(III) Ions and Copper(II). *Inorg. Chem.* **2015**, 54, 2345–2356.
- (32) Price, E. W.; Zeglis, B. M.; Cawthray, J. F.; Lewis, J. S.; Adam, M. J.; Orvig, C. What a Difference a Carbon Makes: H_4 Octapa vs H_4 C3octapa, Ligands for In-111 and Lu-177 Radiochemistry. *Inorg. Chem.* **2014**, 53, 10412–10431.
- (33) Price, E. W.; Cawthray, J. F.; Adam, M. J.; Orvig, C. Modular Syntheses of H_4 Octapa and H_2 Dedpa, and Yttrium Coordination Chemistry Relevant to $^{86}Y/^{90}Y$ Radiopharmaceuticals. *Dalton Trans.* **2014**, 43, 7176–7190.
- (34) Price, E. W.; Zeglis, B. M.; Cawthray, J. F.; Ramogida, C. F.; Ramos, N.; Lewis, J. S.; Adam, M. J.; Orvig, C. Versatile Acyclic Chelate System for ^{111}In and ^{177}Lu Imaging and Therapy. *J. Am. Chem. Soc.* **2013**, 135, 12707–12721.
- (35) Price, E. W.; Edwards, K. J.; Carnazza, K. E.; Carlin, S. D.; Zeglis, B. M.; Adam, M. J.; Orvig, C.; Lewis, J. S. A Comparative Evaluation of the Chelators H_4 Octapa and $CHX-A''$ -DTPA with the Therapeutic Radiometal ^{90}Y . *Nucl. Med. Biol.* **2016**, 43, 566–576.
- (36) Li, L.; Kuo, H.-T.; Wang, X.; Merckens, H.; Colpo, N.; Radchenko, V.; Schaffer, P.; Lin, K.-S.; Bénard, F.; Orvig, C. tBu_4 Octapa-Alkyl-NHS for Metalloradiopeptide Preparation. *Dalton Trans.* **2020**, 49, 7605–7619.
- (37) Ramogida, C. F.; Cawthray, J. F.; Boros, E.; Ferreira, C. L.; Patrick, B. O.; Adam, M. J.; Orvig, C. H_2 CHXDeDpa and H_4 CHXOctapa—Chiral Acyclic Chelating Ligands for $^{67/68}Ga$ and ^{111}In Radiopharmaceuticals. *Inorg. Chem.* **2015**, 54, 2017–2031.
- (38) Tircsó, G.; Regueiro-Figueroa, M.; Nagy, V.; Garda, Z.; Garai, T.; Kálmán, F. K.; Esteban-Gómez, D.; Tóth, É.; Platas-Iglesias, C. Approaching the Kinetic Inertness of Macrocyclic Gadolinium(III)-Based MRI Contrast Agents with Highly Rigid Open-Chain Derivatives. *Chem.—Eur. J.* **2016**, 22, 896–901.
- (39) Rodríguez-Rodríguez, A.; Garda, Z.; Ruscsák, E.; Esteban-Gómez, D.; de Blas, A.; Rodríguez-Blas, T.; Lima, L. M. P.; Beyler, M.; Tripier, R.; Tircsó, G.; Platas-Iglesias, C. Stable Mn^{2+} , Cu^{2+} and Ln^{3+} Complexes with Cyclen-Based Ligands Functionalized with Picolinate Pendant Arms. *Dalton Trans.* **2015**, 44, 5017–5031.
- (40) Helm, L.; Morrow, J. R.; Bond, C. J.; Carniato, F.; Botta, M.; Braun, M.; Baranyai, Z.; Pujales-Paradela, R.; Regueiro-Figueroa, M.; Esteban-Gómez, D.; Platas-Iglesias, C.; Scholl, T. J. Chapter 2. Gadolinium-Based Contrast Agents. In *New Developments in NMR*; Pierre, V. C., Allen, M. J., Eds.; Royal Society of Chemistry: Cambridge, 2017; pp 121–242.
- (41) Regueiro-Figueroa, M.; Esteban-Gómez, D.; de Blas, A.; Rodríguez-Blas, T.; Platas-Iglesias, C. Understanding Stability Trends along the Lanthanide Series. *Chem.—Eur. J.* **2014**, 20, 3974–3981.
- (42) Roca-Sabio, A.; Mato-Iglesias, M.; Esteban-Gómez, D.; Tóth, É.; Blas, A. d.; Platas-Iglesias, C.; Rodríguez-Blas, T. Macrocyclic Receptor Exhibiting Unprecedented Selectivity for Light Lanthanides. *J. Am. Chem. Soc.* **2009**, 131, 3331–3341.
- (43) Hu, A.; MacMillan, S. N.; Wilson, J. J. Macrocyclic Ligands with an Unprecedented Size-Selectivity Pattern for the Lanthanide Ions. *J. Am. Chem. Soc.* **2020**, 142, 13500–13506.
- (44) Thiele, N. A.; Woods, J. J.; Wilson, J. J. Implementing F-Block Metal Ions in Medicine: Tuning the Size Selectivity of Expanded Macrocycles. *Inorg. Chem.* **2019**, 58, 10483–10500.
- (45) Baranyai, Z.; Tei, L.; Giovenzana, G. B.; Kálmán, F. K.; Botta, M. Equilibrium and NMR Relaxometric Studies on the *s*-Triazine-Based Heptadentate Ligand PTDITA Showing High Selectivity for Gd^{3+} Ions. *Inorg. Chem.* **2012**, 51, 2597–2607.
- (46) Woods, J. J.; Unnerstall, R.; Hasson, A.; Abou, D. S.; Radchenko, V.; Thorek, D. L. J.; Wilson, J. J. Stable Chelation of the Uranyl Ion by Acyclic Hexadentate Ligands: Potential Applications for ^{230}U Targeted α -Therapy. *Inorg. Chem.* **2022**, 61, 3337–3350.
- (47) Takács, A.; Napolitano, R.; Purgel, M.; Bényei, A. C.; Zékány, L.; Brücher, E.; Tóth, I.; Baranyai, Z.; Aime, S. Solution Structures, Stabilities, Kinetics, and Dynamics of DO3A and DO3A-Sulphonamide Complexes. *Inorg. Chem.* **2014**, 53, 2858–2872.
- (48) Gündüz, S.; Vibhute, S.; Botár, R.; Kálmán, F. K.; Tóth, I.; Tircsó, G.; Regueiro-Figueroa, M.; Esteban-Gómez, D.; Platas-Iglesias, C.; Angelovski, G. Coordination Properties of GdDO3A-Based Model Compounds of Bioresponsive MRI Contrast Agents. *Inorg. Chem.* **2018**, 57, 5973–5986.
- (49) Cacheris, W. P.; Nickle, S. K.; Sherry, A. D. Thermodynamic Study of Lanthanide Complexes of 1,4,7-Triazacyclononane-*N,N',N''*-Triacetic Acid and 1,4,7,10-Tetraazacyclododecane-*N,N',N'',N'''*-Tetraacetic Acid. *Inorg. Chem.* **1987**, 26, 958–960.

- (50) Supkowski, R. M.; Horrocks, W. D. On the Determination of the Number of Water Molecules, q , Coordinated to Europium(III) Ions in Solution from Luminescence Decay Lifetimes. *Inorg. Chim. Acta.* **2002**, *340*, 44–48.
- (51) Beeby, A.; Clarkson, I. M.; Dickens, R. S.; Faulkner, S.; Parker, D.; Royle, L.; de Sousa, A. S.; Williams, J. A. G.; Woods, M. Non-Radiative Deactivation of the Excited States of Europium, Terbium and Ytterbium Complexes by Proximate Energy-Matched OH, NH and CH Oscillators: An Improved Luminescence Method for Establishing Solution Hydration States. *J. Chem. Soc., Perkin Trans. 2* **1999**, *3*, 493–504.
- (52) Chauvin, A. S.; Gummy, F.; Imbert, D.; Bünzli, J. C. G. Europium and Terbium Tris(Dipicolinates) as Secondary Standards for Quantum Yield Determination. *Spectrosc. Lett.* **2004**, *37*, 517–532.
- (53) Chauvin, A. S.; Gummy, F.; Imbert, D.; Bünzli, J. C. G. Erratum. *Spectrosc. Lett.* **2007**, *40*, 193.
- (54) Werts, M. H. V.; Jukes, R. T. F.; Verhoeven, J. W. The Emission Spectrum and the Radiative Lifetime of Eu^{3+} in Luminescent Lanthanide Complexes. *Phys. Chem. Chem. Phys.* **2002**, *4*, 1542–1548.
- (55) Hancock, R. Macrocyclic Ligands with Pendent Amide and Alcoholic Oxygen Donor Groups. *Coord. Chem. Rev.* **1996**, *148*, 315–347.
- (56) Le Fur, M.; Molnár, E.; Beyler, M.; Fougère, O.; Esteban-Gómez, D.; Rousseaux, O.; Tripier, R.; Tircsó, G.; Platas-Iglesias, C. Expanding the Family of PycLen-Based Ligands Bearing Pendant Picolate Arms for Lanthanide Complexation. *Inorg. Chem.* **2018**, *57*, 6932–6945.
- (57) Chatterton, N.; Bretonnière, Y.; Pécaut, J.; Mazzanti, M. An Efficient Design for the Rigid Assembly of Four Bidentate Chromophores in Water-Stable Highly Luminescent Lanthanide Complexes. *Angew. Chem., Int. Ed.* **2005**, *44*, 7595–7598.
- (58) Guanci, C.; Giovenzana, G.; Lattuada, L.; Platas-Iglesias, C.; Charbonnière, L. J. AMPED. A New Platform for Picolate Based Luminescent Lanthanide Chelates. *Dalton Trans.* **2015**, *44*, 7654–7661.
- (59) Nocton, G. g.; Nonat, A.; Gateau, C.; Mazzanti, M. Water Stability and Luminescence of Lanthanide Complexes of Tripodal Ligands Derived from 1,4,7-Triazacyclononane: Pyridinecarboxamide versus Pyridinecarboxylate Donors. *Helv. Chim. Acta* **2009**, *92*, 2257–2273.
- (60) Bui, A. T.; Beyler, M.; Liao, Y.-Y.; Grichine, A.; Duperray, A.; Mulatier, J.-C.; Guennic, B. L.; Andraud, C.; Maury, O.; Tripier, R. Cationic Two-Photon Lanthanide Bioprobes Able to Accumulate in Live Cells. *Inorg. Chem.* **2016**, *55*, 7020–7025.
- (61) Hamon, N.; Roux, A.; Beyler, M.; Mulatier, J.-C.; Andraud, C.; Nguyen, C.; Maynadier, M.; Bettache, N.; Duperray, A.; Grichine, A.; Brasselet, S.; Gary-Bobo, M.; Maury, O.; Tripier, R. PycLen-Based Ln(III) Complexes as Highly Luminescent Bioprobes for In Vitro and In Vivo One- and Two-Photon Bioimaging Applications. *J. Am. Chem. Soc.* **2020**, *142*, 10184–10197.
- (62) Picot, A.; D'Aléo, A.; Baldeck, P. L.; Grichine, A.; Duperray, A.; Andraud, C.; Maury, O. Long-Lived Two-Photon Excited Luminescence of Water-Soluble Europium Complex: Applications in Biological Imaging Using Two-Photon Scanning Microscopy. *J. Am. Chem. Soc.* **2008**, *130*, 1532–1533.
- (63) Binnemans, K. Interpretation of Europium(III) Spectra. *Coord. Chem. Rev.* **2015**, *295*, 1–45.
- (64) Nonat, A.; Gateau, C.; Fries, P. H.; Mazzanti, M. Lanthanide Complexes of a Picolate Ligand Derived from 1,4,7-Triazacyclononane with Potential Application in Magnetic Resonance Imaging and Time-Resolved Luminescence Imaging. *Chem.—Eur. J.* **2006**, *12*, 7133–7150.
- (65) Nonat, A.; Giraud, M.; Gateau, C.; Fries, P. H.; Helm, L.; Mazzanti, M. Gadolinium(III) Complexes of 1,4,7-Triazacyclononane Based Picolate Ligands: Simultaneous Optimization of Water Exchange Kinetics and Electronic Relaxation. *Dalton Trans.* **2009**, *38*, 8033–8046.
- (66) Nonat, A. M. Complexes de Lanthanides(III) Pour Le Développement de Nouvelles Sondes Magnétiques et Luminescentes. Ph.D. Thesis, Université Joseph-Fourier—Grenoble I, 2007.
- (67) Mason, K.; Harnden, A. C.; Patrick, C. W.; Poh, A. W. J.; Batsanov, A. S.; Suturina, E. A.; Vonci, M.; McInnes, E. J. L.; Chilton, N. F.; Parker, D. Exquisite Sensitivity of the Ligand Field to Solvation and Donor Polarisability in Coordinatively Saturated Lanthanide Complexes. *Chem. Commun.* **2018**, *54*, 8486–8489.
- (68) Dickens, R. S.; Parker, D.; Bruce, J.; Tozer, D. Correlation of Optical and NMR Spectral Information with Coordination Variation for Axially Symmetric Macrocyclic Eu(III) and Yb(III) Complexes: Axial Donor Polarisability Determines Ligand Field and Cation Donor Preference. *Dalton Trans.* **2003**, *7*, 1264–1271.
- (69) Cai, Z.; Wei, C.; Sun, B.; Wei, H.; Liu, Z.; Bian, Z.; Huang, C. Luminescent Europium(III) Complexes Based on Tridentate Isoquinoline Ligands with Extremely High Quantum Yield. *Inorg. Chem. Front.* **2021**, *8*, 41–47.
- (70) Kovacs, D.; Kiraev, S. R.; Phipps, D.; Orthaber, A.; Borbas, K. E. Eu(III) and Tb(III) Complexes of Octa- and Nonadentate Macrocyclic Ligands Carrying Azide, Alkyne, and Ester Reactive Groups. *Inorg. Chem.* **2020**, *59*, 106–117.
- (71) Kovacs, D.; Kocsi, D.; Wells, J. A. L.; Kiraev, S. R.; Borbas, K. E. Electron Transfer Pathways in Photoexcited Lanthanide(III) Complexes of Picolate Ligands. *Dalton Trans.* **2021**, *50*, 4244–4254.
- (72) Doffek, C.; Alzakhem, N.; Bischof, C.; Wahsner, J.; Güden-Silber, T.; Lügger, J.; Platas-Iglesias, C.; Seitz, M. Understanding the Quenching Effects of Aromatic C–H- and C–D-Oscillators in Near-IR Lanthanoid Luminescence. *J. Am. Chem. Soc.* **2012**, *134*, 16413–16423.
- (73) Bertini, I.; Luchinat, C.; Parigi, G. Magnetic Susceptibility in Paramagnetic NMR. *Prog. Nucl. Magn. Reson. Spectrosc.* **2002**, *40*, 249–273.
- (74) Peters, J. A.; Djanashvili, K.; Geraldes, C. F. G. C.; Platas-Iglesias, C. The Chemical Consequences of the Gradual Decrease of the Ionic Radius along the Ln-Series. *Coord. Chem. Rev.* **2020**, *406*, 213146.
- (75) Aime, S.; Barbero, L.; Botta, M.; Ermondi, G. Determination of Metal-Proton Distances and Electronic Relaxation Times in Lanthanide Complexes by Nuclear Magnetic Resonance Spectroscopy. *J. Chem. Soc., Dalton Trans.* **1992**, 225–228.
- (76) Lisowski, J.; Sessler, J. L.; Lynch, V.; Modyi, T. D. ^1H NMR Spectroscopic Study of Paramagnetic Lanthanide(III) Texaphyrins. Effect of Axial Ligation. *J. Am. Chem. Soc.* **1995**, *117*, 2273.
- (77) Lisowski, J.; Ripoli, S.; Di Bari, L. Axial Ligand Exchange in Chiral Macrocyclic Ytterbium(III) Complexes. *Inorg. Chem.* **2004**, *43*, 1388–1394.
- (78) Regueiro-Figueroa, M.; Bensenane, B.; Ruscsák, E.; Esteban-Gómez, D.; Charbonnière, L. J.; Tircsó, G.; Tóth, I.; de Blas, A.; Rodríguez-Blas, T.; Platas-Iglesias, C. Lanthanide DOTA-like Complexes Containing a Picolate Pendant: Structural Entry for the Design of Ln^{III}-Based Luminescent Probes. *Inorg. Chem.* **2011**, *50*, 4125–4141.
- (79) Vipond, J.; Woods, M.; Zhao, P.; Tircsó, G.; Ren, J.; Bott, S. G.; Ogrin, D.; Kiefer, G. E.; Kovacs, Z.; Sherry, A. D. A Bridge to Coordination Isomer Selection in Lanthanide(III) DOTA-Tetraamide Complexes. *Inorg. Chem.* **2007**, *46*, 2584–2595.
- (80) Martins, A. F.; Eliseeva, S. V.; Carvalho, H. F.; Teixeira, J. M. C.; Paula, C. T. B.; Hermann, P.; Platas-Iglesias, C.; Petoud, S.; Tóth, É.; Geraldes, C. F. G. C. A Bis(Pyridine N -Oxide) Analogue of DOTA: Relaxometric Properties of the Gd^{III} Complex and Efficient Sensitization of Visible and NIR-Emitting Lanthanide(III) Cations Including Pr^{III} and Ho^{III}. *Chem.—Eur. J.* **2014**, *20*, 14834–14845.
- (81) Peters, J. A. The Reliability of Parameters Obtained by Fitting of ^1H NMRD Profiles and ^{17}O NMR Data of Potential Gd³⁺-Based MRI Contrast Agents: Fitting of ^1H NMRD Profiles and ^{17}O NMR Data. *Contrast Media Mol. Imaging* **2016**, *11*, 160–168.
- (82) Maigut, J.; Meier, R.; Zahl, A.; Eldik, R. v. Triggering Water Exchange Mechanisms via Chelate Architecture. Shielding of

Transition Metal Centers by Aminopolycarboxylate Spectator Ligands. *J. Am. Chem. Soc.* **2008**, *130*, 14556–14569.

(83) Solomon, I. Relaxation Processes in a System of Two Spins. *Phys. Rev.* **1955**, *99*, 559–565.

(84) Bloembergen, N. Proton Relaxation Times in Paramagnetic Solutions. *J. Chem. Phys.* **1957**, *27*, 572–573.

(85) Bloembergen, N.; Morgan, L. O. Proton Relaxation Times in Paramagnetic Solutions. Effects of Electron Spin Relaxation. *J. Chem. Phys.* **1961**, *34*, 842–850.

(86) Freed, J. H. Dynamic Effects of Pair Correlation Functions on Spin Relaxation by Translational Diffusion in Liquids. II. Finite Jumps and Independent T_1 Processes. *J. Chem. Phys.* **1978**, *68*, 4034–4037.

(87) Swift, T. J.; Connick, R. E. NMR-Relaxation Mechanisms of O^{17} in Aqueous Solutions of Paramagnetic Cations and the Lifetime of Water Molecules in the First Coordination Sphere. *J. Chem. Phys.* **1962**, *37*, 307–320.

(88) Swift, T. J.; Connick, R. E. Erratum: NMR-Relaxation Mechanisms of ^{17}O in Aqueous Solutions of Paramagnetic Cations and the Lifetime of Water Molecules in the First Coordination Sphere. *J. Chem. Phys.* **1964**, *41*, 2553–2554.

(89) Powell, D. H.; Dhubhghaill, O. M. N.; Pubanz, D.; Helm, L.; Lebedev, Y. S.; Schlaepfer, W.; Merbach, A. E. Structural and Dynamic Parameters Obtained from ^{17}O NMR, EPR, and NMRD Studies of Monomeric and Dimeric Gd^{3+} Complexes of Interest in Magnetic Resonance Imaging: An Integrated and Theoretically Self-Consistent Approach¹. *J. Am. Chem. Soc.* **1996**, *118*, 9333–9346.

(90) Halle, B.; Wennerström, H. Interpretation of Magnetic Resonance Data from Water Nuclei in Heterogeneous Systems. *J. Chem. Phys.* **1981**, *75*, 1928–1943.

(91) Yazzev, O. V.; Helm, L. ^{17}O Nuclear Quadrupole Coupling Constants of Water Bound to a Metal Ion: A Gadolinium(III) Case Study. *J. Chem. Phys.* **2006**, *125*, 054503.

(92) Dunand, F. A.; Borel, A.; Merbach, A. E. How Does Internal Motion Influence the Relaxation of the Water Protons in Ln^{III} DOTA-like Complexes? *J. Am. Chem. Soc.* **2002**, *124*, 710–716.

(93) Aime, S.; Botta, M.; Garda, Z.; Kucera, B. E.; Tircso, G.; Young, V. G.; Woods, M. Properties, Solution State Behavior, and Crystal Structures of Chelates of DOTMA. *Inorg. Chem.* **2011**, *50*, 7955–7965.

(94) Caravan, P.; Esteban-Gómez, D.; Rodríguez-Rodríguez, A.; Platas-Iglesias, C. Water Exchange in Lanthanide Complexes for MRI Applications. Lessons Learned over the Last 25 Years. *Dalton Trans.* **2019**, *48*, 11161–11180.

(95) Balogh, E.; Mato-Iglesias, M.; Platas-Iglesias, C.; Tóth, É.; Djanashvili, K.; Peters, J. A.; de Blas, A.; Rodríguez-Blas, T. Pyridine- and Phosphonate-Containing Ligands for Stable Ln Complexation. Extremely Fast Water Exchange on the Gd^{III} Chelates. *Inorg. Chem.* **2006**, *45*, 8719–8728.

(96) Hao, D.; Ai, T.; Goerner, F.; Hu, X.; Runge, V. M.; Tweedle, M. MRI Contrast Agents: Basic Chemistry and Safety. *J. Magn. Reson. Imag.* **2012**, *36*, 1060–1071.

(97) Price, E. W.; Orvig, C. Matching Chelators to Radiometals for Radiopharmaceuticals. *Chem. Soc. Rev.* **2014**, *43*, 260–290.

(98) Garda, Z.; Nagy, V.; Rodríguez-Rodríguez, A.; Pujales-Paradela, R.; Patinec, V.; Angelovski, G.; Tóth, É.; Kálmán, F. K.; Esteban-Gómez, D.; Tripier, R.; Platas-Iglesias, C.; Tircsó, G. Unexpected Trends in the Stability and Dissociation Kinetics of Lanthanide(III) Complexes with Cyclen-Based Ligands across the Lanthanide Series. *Inorg. Chem.* **2020**, *59*, 8184–8195.

(99) Klungness, G. D.; Byrne, R. H. Comparative Hydrolysis Behavior of the Rare Earths and Yttrium: The Influence of Temperature and Ionic Strength. *Polyhedron* **2000**, *19*, 99–107.

(100) Fulmer, G. R.; Miller, A. J. M.; Sherden, N. H.; Gottlieb, H. E.; Nudelman, A.; Stoltz, B. M.; Bercaw, J. E.; Goldberg, K. I. NMR Chemical Shifts of Trace Impurities: Common Laboratory Solvents, Organics, and Gases in Deuterated Solvents Relevant to the Organometallic Chemist. *Organometallics* **2010**, *29*, 2176–2179.

(101) Raiford, D. S.; Fisk, C. L.; Becker, E. D. Calibration of Methanol and Ethylene Glycol Nuclear Magnetic Resonance Thermometers. *Anal. Chem.* **1979**, *51*, 2050–2051.

(102) Meiboom, S.; Gill, D. Modified Spin-Echo Method for Measuring Nuclear Relaxation Times. *Rev. Sci. Instrum.* **1958**, *29*, 688–691.

(103) Micskei, K.; Helm, L.; Brucher, E.; Merbach, A. E. Oxygen-17 NMR Study of Water Exchange on Gadolinium Polyaminopolyacetates $[Gd(DTPA)(H_2O)]^{2-}$ and $[Gd(DOTA)(H_2O)]^-$ Related to NMR Imaging. *Inorg. Chem.* **1993**, *32*, 3844–3850.

(104) Hugi, A. D.; Helm, L.; Merbach, A. E. Water Exchange on Hexa-aquavanadium(III): A Variable-Temperature and Variable-Pressure ^{17}O -NMR Study at 1.4 and 4.7 Tesla. *Helv. Chim. Acta* **1985**, *68*, 508–521.

(105) Irving, H. M.; Miles, M. G.; Pettit, L. D. A Study of Some Problems in Determining the Stoichiometric Proton Dissociation Constants of Complexes by Potentiometric Titrations Using Glass Electrode. *Anal. Chim. Acta* **1967**, *38*, 475–488.

(106) Molnár, E.; Camus, N.; Patinec, V.; Rolla, G. A.; Botta, M.; Tircsó, G.; Kálmán, F. K.; Fodor, T.; Tripier, R.; Platas-Iglesias, C. Picolinate-Containing Macrocyclic Mn^{2+} Complexes as Potential MRI Contrast Agents. *Inorg. Chem.* **2014**, *53*, 5136–5149.

(107) Zekany, L. *PSEQUAD. Computational Methods for the Determination of Formation Constants*; Modern Inorganic Chemistry; Springer: Boston, MA, 1985.

(108) Zhao, Y.; Truhlar, D. G. The M06 Suite of Density Functionals for Main Group Thermochemistry, Thermochemical Kinetics, Noncovalent Interactions, Excited States, and Transition Elements: Two New Functionals and Systematic Testing of Four M06-Class Functionals and 12 Other Functionals. *Theor. Chem. Acc.* **2008**, *120*, 215–241.

(109) Regueiro-Figueroa, M.; Platas-Iglesias, C. Toward the Prediction of Water Exchange Rates in Magnetic Resonance Imaging Contrast Agents: A Density Functional Theory Study. *J. Phys. Chem. A* **2015**, *119*, 6436–6445.

(110) Dolg, M.; Stoll, H.; Savin, A.; Preuss, H. Energy-Adjusted Pseudopotentials for the Rare Earth Elements. *Theor. Chim. Acta* **1989**, *75*, 173–194.

(111) Cao, X.; Dolg, M. Segmented Contraction Scheme for Small-Core Lanthanide Pseudopotential Basis Sets. *J. Mol. Struct.: THEOCHEM* **2002**, *581*, 139–147.

(112) Tomasi, J.; Mennucci, B.; Cammi, R. Quantum Mechanical Continuum Solvation Models. *Chem. Rev.* **2005**, *105*, 2999–3094.

(113) Frisch, M. J.; Trucks, G. W.; Schlegel, H. B.; Scuseria, G. E.; Robb, M. A.; Cheeseman, J. R.; Scalmani, G.; Barone, V.; Petersson, G. A.; Nakatsuji, H.; Li, X.; Caricato, M.; Marenich, A. V.; Bloino, J.; Janesko, B. G.; Gomperts, R.; Mennucci, B.; Hratchian, H. P.; Ortiz, J. V.; Izmaylov, A. F.; Sonnenberg, J. L.; Williams-Young, D.; Ding, F.; Lipparini, F.; Egidi, F.; Goings, J.; Peng, B.; Petrone, A.; Henderson, T.; Ranasinghe, D.; Zakrzewski, V. G.; Gao, J.; Rega, N.; Zheng, G.; Liang, W.; Hada, M.; Ehara, M.; Toyota, K.; Fukuda, R.; Hasegawa, J.; Ishida, M.; Nakajima, T.; Honda, Y.; Kitao, O.; Nakai, H.; Vreven, T.; Throssell, K.; Montgomery, J. A., Jr.; Peralta, J. E.; Ogliaro, F.; Bearpark, M. J.; Heyd, J. J.; Brothers, E. N.; Kudin, K. N.; Staroverov, V. N.; Keith, T. A.; Kobayashi, R.; Normand, J.; Raghavachari, K.; Rendell, A. P.; Burant, J. C.; Iyengar, S. S.; Tomasi, J.; Cossi, M.; Millam, J. M.; Klene, M.; Adamo, C.; Cammi, R.; Ochterski, J. W.; Martin, R. L.; Morokuma, K.; Farkas, O.; Foresman, J. B.; Fox, D. J. *Gaussian16*, Revision C.01, 2016.

(114) Neese, F. Prediction of Molecular Properties and Molecular Spectroscopy with Density Functional Theory: From Fundamental Theory to Exchange-Coupling. *Coord. Chem. Rev.* **2009**, *253*, 526–563.

(115) Neese, F. The ORCA Program System. *Wiley Interdiscip. Rev.: Comput. Mol. Sci.* **2012**, *2*, 73–78.

(116) Neese, F. Software Update: The ORCA Program System, Version 4.0. *Wiley Interdiscip. Rev.: Comput. Mol. Sci.* **2018**, *8*, No. e1327.

(117) Visscher, L.; Dyall, K. G. Dirac–Fock Atomic Electronic Structure Calculations Using Different Nuclear Charge Distributions. *At. Data Nucl. Data Tables* **1997**, *67*, 207–224.

(118) Tao, J.; Perdew, J. P.; Staroverov, V. N.; Scuseria, G. E. Climbing the Density Functional Ladder: Nonempirical Meta–Generalized Gradient Approximation Designed for Molecules and Solids. *Phys. Rev. Lett.* **2003**, *91*, 146401.

(119) Esteban-Gómez, D.; de Blas, A.; Rodríguez-Blas, T.; Helm, L.; Platas-Iglesias, C. Hyperfine Coupling Constants on Inner-Sphere Water Molecules of Gd^{III}-Based MRI Contrast Agents. *ChemPhysChem* **2012**, *13*, 3640–3650.

(120) Kossmann, S.; Kirchner, B.; Neese, F. Performance of Modern Density Functional Theory for the Prediction of Hyperfine Structure: Meta-GGA and Double Hybrid Functionals. *Mol. Phys.* **2007**, *105*, 2049–2071.

(121) Reiher, M. Douglas–Kroll–Hess Theory: A Relativistic Electrons-Only Theory for Chemistry. *Theor. Chem. Acc.* **2006**, *116*, 241–252.

(122) Barysz, M.; Sadlej, A. J. Two-Component Methods of Relativistic Quantum Chemistry: From the Douglas–Kroll Approximation to the Exact Two-Component Formalism. *J. Mol. Struct.: THEOCHEM* **2001**, *573*, 181–200.

(123) Aravena, D.; Neese, F.; Pantazis, D. A. Improved Segmented All-Electron Relativistically Contracted Basis Sets for the Lanthanides. *J. Chem. Theory Comput.* **2016**, *12*, 1148–1156.

(124) Weigend, F.; Ahlrichs, R. Balanced Basis Sets of Split Valence, Triple Zeta Valence and Quadruple Zeta Valence Quality for H to Rn: Design and Assessment of Accuracy. *Phys. Chem. Chem. Phys.* **2005**, *7*, 3297.

(125) Kossmann, S.; Neese, F. Comparison of Two Efficient Approximate Hartree–Fock Approaches. *Chem. Phys. Lett.* **2009**, *481*, 240–243.

(126) Neese, F.; Wennmohs, F.; Hansen, A.; Becker, U. Efficient, Approximate and Parallel Hartree–Fock and Hybrid DFT Calculations. A ‘Chain-of-Spheres’ Algorithm for the Hartree–Fock Exchange. *Chem. Phys.* **2009**, *356*, 98–109.

(127) Stoychev, G. L.; Auer, A. A.; Neese, F. Automatic Generation of Auxiliary Basis Sets. *J. Chem. Theory Comput.* **2017**, *13*, 554–562.

(128) Weigend, F. Accurate Coulomb-Fitting Basis Sets for H to Rn. *Phys. Chem. Chem. Phys.* **2006**, *8*, 1057–1065.

(129) Marenich, A. V.; Cramer, C. J.; Truhlar, D. G. Universal Solvation Model Based on Solute Electron Density and on a Continuum Model of the Solvent Defined by the Bulk Dielectric Constant and Atomic Surface Tensions. *J. Phys. Chem. B* **2009**, *113*, 6378–6396.

Recommended by ACS

Binuclear Lanthanide Complexes Based on 4-Picoline-*N*-oxide: From Sensitized Luminescence to Single-Molecule Magnet Characteristics

Senthil Kumar Kuppasamy, Mario Ruben, *et al.*

JANUARY 16, 2023

CRYSTAL GROWTH & DESIGN

READ 

Spinolate Lanthanide Complexes for High Circularly Polarized Luminescence Metrics in the Visible and Near-Infrared

Bre-Anna N. Willis, Gaël Ung, *et al.*

NOVEMBER 29, 2022

JOURNAL OF THE AMERICAN CHEMICAL SOCIETY

READ 

Lanthanide and Actinide Ion Complexes Containing Organic Ligands Investigated by Surface-Enhanced Infrared Absorption Spectroscopy

Sakiko Hirata, Yoshiya Inokuchi, *et al.*

DECEMBER 22, 2022

INORGANIC CHEMISTRY

READ 

Luminescence of Macrocyclic Mononuclear Dy^{III} Complexes and Their Immobilization on Functionalized Silicon-Based Surfaces

Yolimar Gil, Evgenia Spodine, *et al.*

OCTOBER 05, 2022

INORGANIC CHEMISTRY

READ 